

# CORRELATED $\pi\rho$ EXCHANGE IN THE $NN$ INTERACTION

G. Janssen, K. Holinde, and J. Speth  
*Institut für Kernphysik, Forschungszentrum Jülich GmbH,  
D-52425 Jülich, Germany*

We evaluate the contribution to the nucleon-nucleon interaction due to correlated  $\pi\rho$  exchange in the  $\pi$ ,  $\omega$ , and  $A_1/H_1$  channels by means of dispersion-theoretic methods based on a realistic meson exchange model for the interaction between  $\pi$  and  $\rho$  mesons. These processes have substantial effects: In the pionic channel it counterbalances the suppression generated by a soft  $\pi NN$  form factor of monopole type with a cutoff mass of about 1 GeV; in the  $\omega$ -channel it provides nearly half of the empirical repulsion, leaving little room for explicit quark-gluon effects.

21.30.+y, 13.75.Cs

## I. INTRODUCTION

The study of meson-meson systems and their role in low and medium energy physics is of twofold interest. First, from a more basic viewpoint, the investigation of meson-meson interactions provides important information about the fundamental structure of strong interactions. This is especially true for the lightest system consisting of two pions.  $\pi\pi$  scattering at low energies is determined by chiral symmetry and therefore plays a dominant role in chiral perturbation theory. For higher energies the study of  $\pi\pi$  as well as  $\pi\eta$  scattering (including the coupling to the  $K\bar{K}$  channel) provides essential information on the nature of scalar resonances. Within a meson exchange  $\pi\pi$  ( $\pi\eta$ )/ $K\bar{K}$  model the  $f_0(980)$  turns out to be a  $K\bar{K}$  bound state and the  $a_0(980)$  a  $K\bar{K}$  threshold effect [1]. Second, the inclusion of meson-meson correlations is mandatory for numerous hadronic processes. In models of nucleons consisting of a quark-gluon ‘core’ and a meson cloud, meson-meson couplings have a large impact on the structure of nucleon form factors. In meson-exchange models of the  $NN$  interaction, which essentially include pseudoscalar and vector mesons, one has for consistency not only to include the meson-nucleon, but also the meson-meson interaction. Indeed, the correlated  $2\pi$ -exchange contribution is of outstanding importance, providing the main part of the intermediate-range attraction.

In this work we want to demonstrate the important role of the contribution to the nucleon-nucleon [2] interaction provided by the exchange of a correlated  $\pi\rho$  pair (A corresponding letter has already been published [3]). The starting points are open questions concerning the structure of the  $\pi NN$  vertex. Besides the coupling constant, the  $\pi NN$  vertex function (like all baryon-baryon meson vertices) contains a form factor parametrizing the extended hadron structure and characterized, in a monopole parametrization, by a cutoff mass  $\Lambda_{\pi NN}$ . Within the (full) Bonn potential, the best fit to the  $NN$  data requires a value of  $\Lambda_{\pi NN} = 1.3$  GeV; the resulting form factor modifies the one-pion-exchange potential for small distances ( $r \leq 1$  fm) only. This ensures a tensor force which is strong enough to reproduce the deuteron properties, especially the D/S ratio and the quadrupole moment [4,5]. However such a hard form factor is in contradiction to information from other sources [6–9], which all favor a considerably lower value of  $\Lambda_{\pi NN} \simeq 0.8$  GeV, i.e. a rather ‘soft’ form factor. Obviously the solution of this problem requires the inclusion of additional (short ranged) tensor contributions in the Bonn potential, which compensate for the effect of such a soft  $\pi NN$  form factor. The exchange of a correlated  $\pi\rho$  pair is a natural candidate for such a contribution. Indeed, the inclusion of uncorrelated  $\pi\rho$  processes in the full Bonn potential already led to a reduction of the  $\pi NN$  cutoff mass from 1.75 GeV (in the framework of a simple one-boson-exchange model (OBEPT) [2] defined likewise in time-ordered perturbation theory) to 1.3 GeV. Thus a further reduction of this value is to be expected if correlated  $\pi\rho$  exchange is included. This is anyway required within the strategy advocated in the full Bonn potential: namely to group  $\pi\pi$  and corresponding  $\pi\rho$  contributions together because of their counterstructure in the tensor channel. However, while the Bonn potential contains already correlated  $\pi\pi$  exchange (in terms of sharp mass  $\sigma'$  exchange), the corresponding  $\pi\rho$  process is not included so far.

The evaluation of correlated  $\pi\rho$  exchange (Fig. 1) requires the knowledge of the interaction between  $\pi$  and  $\rho$  mesons. We have recently derived a corresponding meson-theoretical model [10] for  $\pi\rho$  scattering which provides good agreement with the existing empirical information. It is, however, not completely crossing symmetric, so that a direct evaluation of Fig. 1(d) based on this  $\pi\rho$  interaction is not possible. Therefore, as in the  $\pi\pi$  case [11], we first evaluate the amplitude  $N\bar{N} \rightarrow \pi\rho \rightarrow N\bar{N}$  including  $\pi\rho$  correlations. In a second step we use dispersion-theoretic methods to transform this amplitude into the  $s$  ( $NN$ ) channel and in this way obtain the contribution of Fig. 1(d).

A main result will be that the exchange of a correlated  $\pi\rho$  pair indeed generates a contribution to the  $NN$  potential

of sizable strength. In the pionic channel it leads to a tensor force component which is strong enough to cancel the effect of a soft form factor with  $\Lambda_{\pi NN} \simeq 1$  GeV. Moreover, it provides nearly half of the empirical repulsion in the  $\omega$ -channel.

The structure of the paper is as follows: Sect. II provides the basic formalism, together with our model for the  $N\bar{N} \rightarrow \pi\rho$  amplitude; Sect. III presents and discusses the results, in the various  $(\pi, \omega, A_1/H_1)$  channels considered; finally, Sect. IV contains some concluding remarks.

## II. FORMALISM

In the following we outline the formalism which is used to evaluate the correlated  $\pi\rho$  exchange contribution to the  $NN$  interaction.

### A. Dispersion relation for the $NN \rightarrow NN$ amplitude

For  $NN \rightarrow NN$  and  $N\bar{N} \rightarrow N\bar{N}$  scattering the field theoretical scattering amplitude  $T$  is related to the standard  $S$ -matrix by

$$S_{fi} = \delta_{fi} - i(2\pi)^{-2} \delta^{(4)}(p'_1 + p'_2 - p_1 - p_2) \left( \frac{m_N^4}{E'_1 E'_2 E_1 E_2} \right)^{\frac{1}{2}} T_{fi} . \quad (1)$$

If we neglect isospin for the moment, the  $s$ -channel ( $NN \rightarrow NN$ ) amplitude can be written as

$$T_s(p'_1, p'_2; p_1, p_2) = \bar{u}(p'_1, \lambda'_1) \bar{u}(p'_2, \lambda'_2) \hat{T} u(p_1, \lambda_1) u(p_2, \lambda_2) , \quad (2)$$

where

$$u(p, \lambda) = \sqrt{\frac{E(p) + m_N}{2m_N}} \left( \frac{1}{\frac{2\lambda p}{E(p) + m_N}} \right) |\lambda \rangle \quad (3)$$

is a Dirac helicity spinor normalized to  $\bar{u}u = 1$ . (The spin dependence is suppressed on the left hand side of Eq. (2).) For on-shell scattering,  $\hat{T}$  can be expressed as a linear combination of five invariant operators  $\hat{C}_j$ ; the expansion coefficients  $c_j$  are scalar functions of the Mandelstam variables  $s \equiv (p_1 + p_2)^2$  and  $t \equiv (p'_1 - p_1)^2$ . ( $u$  is not independent, but given by  $u = 4m_N^2 - s - t$ .)  $\hat{T}$  can then be written as

$$\hat{T} = \sum_{j=1}^5 c_j(t, s) \hat{C}_j . \quad (4)$$

In contrast to our former work dealing with correlated  $\pi\pi$  exchange [11] we now use, instead of the so-called perturbative invariants (see Ref. [11]) the Fermi-invariants

$$\begin{aligned} S &= (I)^{(1)} (I)^{(2)} \\ P &= (\gamma_5)^{(1)} (\gamma_5)^{(2)} \\ V &= (\gamma^\mu)^{(1)} (\gamma_\mu)^{(2)} \\ A &= (\gamma_5 \gamma^\mu)^{(1)} (\gamma_5 \gamma_\mu)^{(2)} \\ T &= (\sigma^{\mu\nu})^{(1)} (\sigma_{\mu\nu})^{(2)} . \end{aligned} \quad (5)$$

where  $\sigma_{\mu\nu} \equiv \frac{i}{2} [\gamma_\mu, \gamma_\nu]$ .

Correspondingly, the amplitude for the  $t$ -channel ( $N\bar{N} \rightarrow N\bar{N}$ ) process defined in Fig. 2 then reads

$$T_t(-p'_1, p'_2; p_1, -p_2) = \bar{v}(-p'_1, \bar{\lambda}'_1) \bar{u}(p'_2, \lambda'_2) \hat{T} v(p_1, \lambda_1) u(-p_2, \bar{\lambda}_2) . \quad (6)$$

Here

$$v(-p, \lambda) = \sqrt{\frac{E(p) + m_N}{2m_N}} \left( \frac{p}{E(p) + m_N} \right) | -\lambda \rangle \quad (7)$$

is the Dirac spinor for an antiparticle. Due to crossing symmetry  $\hat{T}$  can be represented in the same way as before (Eq. (4)), with precisely the same functions  $c_j$ , however in a different  $s, t$  domain obtained by replacing  $p'_1$  by  $-p'_1$  and  $p_2$  by  $-p_2$ .

The functions  $c_j$  arising from (correlated)  $\pi\rho$  exchange are assumed to fulfill a dispersion relation over the unitarity cut,

$$c_j(t, s) = \frac{1}{\pi} \int_{(m_\pi + m_\rho)^2}^{\infty} \frac{\text{Im } c_j(t', s)}{t' - t - i\epsilon} dt' . \quad (8)$$

(Throughout we take the  $\rho$  to be a stable particle with  $m_\rho = 769$  MeV.) Thus the  $c_j$  can be determined if their imaginary part is known in the pseudophysical region ( $t' \geq (m_\pi + m_\rho)^2$ ) of the  $t$ -channel reaction and for  $s \geq 4m_N^2$ .

## B. Determination of the spectral functions from unitarity

The required information about the spectral functions  $\rho_j(t', s) \equiv \text{Im } c_j(t', s)$  can be obtained from the relevant unitarity relation (cf. Fig. 3)

$$i \langle N\bar{N} | \hat{T} - \hat{T}^\dagger | N\bar{N} \rangle = \sum_{\pi\rho} \Omega_{\pi\rho} \langle N\bar{N} | t^\dagger | \pi\rho \rangle \langle \pi\rho | t | N\bar{N} \rangle \delta^{(4)}(k_1 + k_2 + p'_1 - p_1) \quad (9)$$

where  $\Omega_{\pi\rho}$  is a  $\pi\rho$  phase-space factor. We first do a partial wave decomposition,

$$\begin{aligned} T_t(\mathbf{p}' \lambda'_N \lambda'_{\bar{N}}; \mathbf{p} \lambda_N \lambda_{\bar{N}}; \sqrt{t}) &= \frac{1}{4\pi} \sum_J (2J+1) d_{\lambda\lambda'}^J(\cos\vartheta) T_t^J(p' \lambda'_N \lambda'_{\bar{N}}; p \lambda_N \lambda_{\bar{N}}; \sqrt{t}) \\ t(\mathbf{k} \lambda_\rho; \mathbf{p} \lambda_N \lambda_{\bar{N}}; \sqrt{t}) &= \frac{1}{4\pi} \sum_J (2J+1) d_{\lambda\bar{\lambda}}^J(\cos\bar{\vartheta}) t^J(k \lambda_\rho; p \lambda_N \lambda_{\bar{N}}; \sqrt{t}) \end{aligned} \quad (10)$$

with

$$\lambda' \equiv \lambda'_N - \lambda'_{\bar{N}}, \quad \bar{\lambda} \equiv \lambda_\rho - \lambda_\pi = \lambda_\rho, \quad \lambda \equiv \lambda_N - \lambda_{\bar{N}}, \quad (11)$$

$\mathbf{p}, \mathbf{p}', \mathbf{k}$  being the relative 3-momenta in the center-of-mass (cm) system and the angles  $\vartheta = \angle(\mathbf{p}, \mathbf{p}')$ ,  $\bar{\vartheta} = \angle(\mathbf{p}, \mathbf{k})$ . After transformation into LSJ basis Eq. (9) goes into

$$\begin{aligned} &\text{Im}[T_t^J(p_0, L' S'; p_0, L S; \sqrt{t})] \\ &= -C \sum_{L\pi\rho} [t^J(k_0, L\pi\rho 1; p_0, L' S'; \sqrt{t})]^\dagger t^J(k_0, L\pi\rho 1; p_0, L S; \sqrt{t}) \equiv {}^J N(L' S'; L S) \end{aligned} \quad (12)$$

where  $C \equiv k_0 / (32\pi^2 \sqrt{t})$  and  $p_0, k_0$  denote the on-shell momenta of the  $N\bar{N}$  and  $\pi\rho$  system, respectively.

As for the  $2\pi$ -exchange case, we want to restrict ourselves to the  $J = 0, 1$   $\pi\rho$  exchange contributions, which act in channels corresponding to the quantum numbers of the pion ( $J = 0$ ), and the  $\omega, A_1$ , and  $H_1$  meson ( $J = 1$ ). Table I shows the quantum numbers and possible transitions from the  $N\bar{N}$  to the  $\pi\rho$  system obtained from the conditions

$$(-1)^{L_{N\bar{N}}+1} = P_\pi P_\rho (-1)^{L_{\pi\rho}} = (-1)^{L_{\pi\rho}} \quad (13)$$

$$(-1)^{L_{N\bar{N}}+S_{N\bar{N}}+I} = G_\pi G_\rho = -1 \quad (14)$$

due to parity and G-parity conservation. We therefore obtain for the different relevant channels

$$\begin{aligned} {}^0 N(00; 00) &= -C(t_{0+}^0)^\dagger t_{0+}^0 && \pi \\ \left. \begin{aligned} {}^1 N(01; 01) &= -C(t_{-1}^1)^\dagger t_{-1}^1 \\ {}^1 N(21; 01) &= -C(t_{+1}^1)^\dagger t_{-1}^1 \\ {}^1 N(01; 21) &= -C(t_{-1}^1)^\dagger t_{+1}^1 \\ {}^1 N(21; 21) &= -C(t_{+1}^1)^\dagger t_{+1}^1 \end{aligned} \right\} \omega && (15) \\ {}^1 N(11; 11) &= -C[(t_{1-}^1)^\dagger t_{1-}^1 + (t_{1+}^1)^\dagger t_{1+}^1] && A_1 \\ {}^1 N(10; 10) &= -C[(t_{0-}^1)^\dagger t_{0-}^1 + (t_{0+}^1)^\dagger t_{0+}^1] && H_1 \end{aligned}$$

The knowledge of  $^J N$  determines the spectral functions. With the help of Appendix A, we have explicitly

$$\begin{aligned}
\rho_P^\pi(s, t) &= -\frac{1}{8\pi\beta^2} {}^0 N(00; 00) \\
\rho_{\{S, V, T, A\}}^\pi(s, t) &= 0 \\
\rho_S^\omega(s, t) &= \frac{1}{16\alpha^2\pi\beta} \cos\vartheta \\
&\quad [\sqrt{2}(\beta-1)^2 {}^1 N(01; 21) + (2\beta^2 + 5\beta + 2) {}^1 N(21; 21) - 2(\beta-1)^2 {}^1 N(01; 01)] \\
\rho_V^\omega(s, t) &= -\frac{1}{16\alpha^2\pi\beta} [\sqrt{2}(2\beta+1) {}^1 N(01; 21) + (\beta^2 + 2) {}^1 N(21; 21) + 2(\beta-1) {}^1 N(01; 01)] \\
\rho_T^\omega(s, t) &= \frac{1}{128\alpha^2\pi\beta^2 m_N^2} t \\
&\quad [\sqrt{2}(\beta+2) {}^1 N(01; 21) + (2\beta+1) {}^1 N(21; 21) - 2(\beta-1) {}^1 N(01; 01)] \\
\rho_P^\omega(s, t) &= \frac{1}{16\pi\beta^2} \cos\vartheta [\sqrt{2}(\beta+2) {}^1 N(01; 21) + (2\beta+1) {}^1 N(21; 21) - 2(\beta-1) {}^1 N(01; 01)] \\
\rho_A^\omega(s, t) &= 0 \\
\rho_P^{A_1}(s, t) &= -\frac{3}{16\alpha^2\pi\beta^2} {}^1 N(11; 11) \\
\rho_A^{A_1}(s, t) &= -\frac{3}{16\alpha^2\pi} {}^1 N(11; 11) \\
\rho_{\{S, V, T\}}^{A_1}(s, t) &= 0 \\
\rho_P^{H_1}(s, t) &= -\frac{3}{8\pi\beta^2} \cos\vartheta {}^1 N(10; 10) \\
\rho_{\{S, V, T, A\}}^{H_1}(s, t) &= 0
\end{aligned} \tag{16}$$

with  $\beta^2 \equiv E^2(p)/m_N^2$  and  $\alpha^2 \equiv \beta^2 - 1$ .

### C. Microscopic model for the $N\bar{N} \rightarrow \pi\rho$ process

The determination of the spectral functions  $\rho_i$  requires the knowledge of the transition amplitude  $t_{N\bar{N} \rightarrow \pi\rho}$  including  $\pi\rho$  correlations. In our dynamical model whose structure is visualized in Fig. 4 this quantity is obtained from

$$t_{N\bar{N} \rightarrow \pi\rho} = v_{N\bar{N} \rightarrow \pi\rho} + v_{N\bar{N} \rightarrow \pi\rho} G_{\pi\rho} T_{\pi\rho \rightarrow \pi\rho}, \tag{17}$$

where  $v_{N\bar{N} \rightarrow \pi\rho}$  is the transition potential specified later,  $G_{\pi\rho}$  is chosen to be the Blankenbecler-Sugar [12] propagator of the  $\pi\rho$  system, and  $T_{\pi\rho \rightarrow \pi\rho}$  is the  $\pi\rho \rightarrow \pi\rho$  amplitude essentially taken from the dynamical model [10]. After partial wave decomposition Eq. (17) reads more explicitly, in the helicity state basis,

$$\begin{aligned}
t^J(k\lambda_\rho; p\lambda_N\lambda_{\bar{N}}; \sqrt{t}) &= v^J(k\lambda_\rho; p\lambda_N\lambda_{\bar{N}}; \sqrt{t}) \\
&+ \sum_{\lambda'_\rho} \int_0^\infty dk' k'^2 \frac{\omega_\rho(k') + \omega_\pi(k')}{(2\pi)^3 2\omega_\rho(k')\omega_\pi(k')} \frac{v^J(k'\lambda'_\rho; p\lambda_N\lambda_{\bar{N}}; \sqrt{t}) T^J(k\lambda_\rho; k'\lambda'_\rho; \sqrt{t})}{t - (\omega_\rho(k') + \omega_\pi(k'))^2}.
\end{aligned} \tag{18}$$

#### 1. The transition potential $v_{N\bar{N} \rightarrow \pi\rho}$ .

Our model for the transition potential  $v_{N\bar{N} \rightarrow \pi\rho}$  is based on nucleon and  $\Delta$  exchange, together with an  $\omega$  pole term (Fig. 5). In principle, further pole terms exist in the channels considered in this work which are, however, not included

in the present calculations for the following reasons: In case of the pion, its mass lies far below the  $\pi\rho$  threshold so that such a diagram has a negligible influence on the dispersion integral, Eq. (8). In case of the  $A_1$  and  $H_1$  little is known about their coupling strength to the nucleon. On the other hand, the (bare)  $\omega NN$  coupling constant can be fixed by adjusting the final result to the empirical  $NN$  repulsion (see below).

The starting point for the evaluation of the corresponding potential expressions is the set of interaction Lagrangians

$$\begin{aligned}
\mathcal{L}_{\pi NN} &= \frac{f_{\pi NN}}{m_\pi} \bar{\psi} \gamma^5 \gamma^\mu \vec{\tau} \partial_\mu \vec{\pi} \psi \\
\mathcal{L}_{\rho NN} &= g_{\rho NN} \bar{\psi} \left[ \gamma^\mu \vec{\tau} \psi \vec{\rho}_\mu + \frac{\kappa}{4m_N} \sigma^{\mu\nu} \vec{\tau} (\partial_\mu \vec{\rho}_\nu - \partial_\nu \vec{\rho}_\mu) \right] \psi \\
\mathcal{L}_{\pi\Delta N} &= \frac{f_{\pi\Delta N}}{m_\pi} \bar{\psi} \vec{T} \psi_\mu \partial^\mu \vec{\pi} + h.c. \\
\mathcal{L}_{\rho\Delta N} &= \frac{f_{\rho\Delta N}}{m_\rho} \bar{\psi} i \gamma^5 \gamma^\mu \vec{T} \psi^\nu (\partial_\mu \vec{\rho}_\nu - \partial_\nu \vec{\rho}_\mu) + h.c. \\
\mathcal{L}_{\omega NN} &= g_{\omega NN} \bar{\psi} \gamma^\mu \omega_\mu \psi \\
\mathcal{L}_{\omega\pi\rho} &= g_{\omega\pi\rho} \epsilon^{\mu\nu\sigma\tau} \partial_\mu \omega_\nu \partial_\sigma \vec{\rho}_\tau \vec{\pi}
\end{aligned} \tag{19}$$

We then obtain for the structure of the potential matrix elements nucleon exchange:

$$v_s = i f F^2 \frac{f_{NN\pi} g_{NN\rho}}{m_\pi} \frac{\bar{v}(q_2) \left\{ \gamma^5 \not{k}_2 [\not{p}_x + m_N] (\not{\epsilon}^* - \frac{\kappa}{4m_N} \not{k}_1 \not{\epsilon}^* + \frac{\kappa}{4m_N} \not{\epsilon}^* \not{k}_1) \right\} u(q_1)}{p_x^2 - m_N^2} \tag{20}$$

$\Delta$  exchange:

$$\begin{aligned}
v_s &= -i f F^2 \frac{f_{N\Delta\pi} g_{N\Delta\rho}}{m_\pi m_\rho} \bar{v}(q_2) (k_2)_\mu S^{\mu\nu} \gamma^5 \gamma^\sigma [(k_1)_\nu \epsilon_\sigma^* - (k_1)_\sigma \epsilon_\nu^*] u(q_1) \\
S^{\mu\nu} &= \frac{\not{p}_x + m_\Delta}{p_x^2 - m_\Delta^2} \left\{ -g^{\mu\nu} + \frac{1}{3} \gamma^\mu \gamma^\nu + \frac{2}{3m_\Delta^2} p_x^\mu p_x^\nu - \frac{1}{3m_\Delta} (p_x^\mu p_x^\nu - p_x^\nu p_x^\mu) \right\}
\end{aligned} \tag{21}$$

$\omega$  exchange:

$$v_t = -f F^2 \frac{g_{\pi\rho\omega}^{(0)} g_{NN\omega}^{(0)}}{m_\omega} \frac{\sqrt{t}}{p_x^2 - (m_\omega^{(0)})^2} \epsilon^{0\nu\sigma\tau} (k_1)_\sigma \epsilon_\tau^* \bar{v}(q_2) \gamma_\nu u(q_1) \tag{22}$$

where  $k_1$  ( $k_2$ ) and  $q_1$  ( $q_2$ ) denote the four-momenta of the  $\rho$  ( $\pi$ ) and nucleon (antinucleon), respectively.  $p_x$  is the momentum of the exchanged particle; for the  $\omega$  exchange term, in the cm system,  $p_x = (\sqrt{t}, 0)$ .  $\epsilon^*$  is the polarization vector for the outgoing  $\rho$  meson.  $F^2$  denotes the product of vertex form factors, for which we used

$$\begin{aligned}
s\text{-channel} : \quad F^2 &= \left( \frac{2\Lambda_{\pi NX}^2 - M_X^2}{2\Lambda_{\pi NX}^2 - p_x^2} \right)^2 \left( \frac{2\Lambda_{\rho NX}^2 - M_X^2}{2\Lambda_{\pi NX}^2 - p_x^2} \right)^2 \\
t\text{-channel} : \quad F^2 &= \left( \frac{\Lambda_{\pi\rho X}^2 + m_X^2}{\Lambda_{\pi\rho X}^2 + [\omega_\pi(k) + \omega_\rho(k)]^2} \right)^2 \left( \frac{2\Lambda_{NNX}^2 + m_X^2}{2\Lambda_{NNX}^2 + 4E(p_x)^2} \right)^2,
\end{aligned} \tag{23}$$

where  $X$  stands for the exchanged particle.  $f$  denotes the isospin factor; corresponding values are given in Table II. The coupling constants are either experimentally known or fixed from our former studies. An exception is the bare  $\omega NN$  coupling  $g_{\omega NN}^{(0)}$  which, as mentioned before, will be fixed later. Values for coupling constants and cutoff masses used are given in Table III. [The  $s$ -channel cutoff masses have been adjusted to reproduce the overall strength of

$N\bar{N} \rightarrow \pi\rho$  potential used in earlier studies [13]. This potential produces good agreement with empirical information above the  $N\bar{N}$  threshold, but is based on a different off-shell behavior (time-ordered perturbation theory rather than BbS.) The zero-th components of momenta are determined by the BbS reduction [14] to be  $q_1^0 = q_2^0 = \sqrt{t}/2$ ,  $k_1^0 = \frac{1}{2}[\sqrt{t} + \omega_\rho(k) - \omega_\pi(k)]$ , and  $k_2^0 = \frac{1}{2}[\sqrt{t} + \omega_\pi(k) - \omega_\rho(k)]$ . The potential matrix elements are then decomposed into LSJ partial waves in the standard way. Further  $u$ -channel diagrams arising from  $N$  and  $\Delta$  exchange can be taken into account by adding a factor of 2 in the (partial wave)  $s$ -channel contributions.

## 2. The amplitude $T_{\pi\rho \rightarrow \pi\rho}$ .

Our model for the correlation amplitude  $T_{\pi\rho \rightarrow \pi\rho}$  [10] is generated from the three-dimensional BbS [12] scattering equation

$$T(\mathbf{k}', \mathbf{k}; E) = V(\mathbf{k}', \mathbf{k}; E) + \int d^3 k'' V(\mathbf{k}', \mathbf{k}''; E) G(\mathbf{k}''; E) T(\mathbf{k}'', \mathbf{k}; E), \quad (24)$$

( $\mathbf{k}, \mathbf{k}', \mathbf{k}''$  are corresponding cm relative momenta) with the potential  $V$  containing the diagrams shown in Fig. 6. It contains, besides non-pole pieces, pole terms with bare parameters (masses, coupling constants) which are renormalized by the iteration in Eq. (24) and in this way acquire their physical properties. Basic interaction Lagrangians have been taken from the nonlinear  $\sigma$ -model in the meson sector where the vector mesons are introduced as gauge bosons of a hidden  $SU(2)$  or  $SU(3)$  symmetry. In this way one obtains the coupling of the  $\rho$  to the  $\pi$  meson and to itself, i.e.  $\mathcal{L}_{\pi\pi\rho}$  and  $\mathcal{L}_{\rho\rho\rho}$ , with a unified value for the coupling constants. Note that we have left out a corresponding pion pole term. The reason is the very small pion mass lying far below the  $\pi\rho$  threshold, so that such a diagram should have a negligible influence in the dispersion integral, Eq. (8).

In addition to the model presented in Ref. [10] the present calculations include the  $H_1$  ( $J^P = 1^+, I^G = 0^-$ ) channel; therefore  $V$  now contains an  $H_1$ -pole term. The corresponding expression is analogous to the  $A_1$ -term, see [10], with the isospin factor  $f = 3\delta_{I,0}$ , bare coupling constant  $(g_{H_1\pi\rho}^{(0)})^2/4\pi = 1.3$  and bare mass  $m_{H_1}^{(0)} = 1100$  MeV. As Fig. 7 shows, we obtain a reasonable description of the  $H_1$  mass distribution, although compared to the  $A_1$  case the model underestimates the empirical situation somewhat. Still, the rough agreement should be sufficient to estimate the relevance of the  $H_1$  channel for the correlated  $\pi\rho$  exchange  $NN$  interaction.

## D. $NN$ interaction arising from correlated $\pi\rho$ exchange

In the last section we specified the dynamical model for the  $N\bar{N} \rightarrow \pi\rho$  amplitude, which yields the spectral functions  $\rho(s, t)$ , Eq. (17). The dispersion integral, Eq. (8), then determines the invariant amplitudes  $c_j(t, s; t < 0)$  and thus the scattering operator  $\hat{T}$  (Eq. (4)). The various  $NN$  potential contributions are then obtained by sandwiching  $\hat{T}$  between in- and outgoing spinors (cf. Eq. (2)).

Such a calculation can be directly pursued for the  $\pi$  and  $A_1$  channel since these spectral functions do not depend on  $\cos\vartheta$ , which is, in terms of the Mandelstam variables,

$$\cos\vartheta = \frac{4m_N^2 - t - 2s}{t - 4m_N^2} = \frac{u - s}{t - 4m_N^2}. \quad (25)$$

When transforming into the  $NN$  channel, corresponding values for  $s > 4m_N^2$  have to be inserted, and, in principle, the  $t$ -dependence in  $\cos\vartheta$  should be integrated over in the dispersion integral. However, it is then not guaranteed that the typical structure of  $s$ -channel vector meson exchange is obtained. Namely, starting from the conventional vector meson Lagrangian,

$$\mathcal{L} = g\bar{\psi}\gamma^\mu\psi V_\mu + f/4m_N\bar{\psi}\sigma^{\mu\nu}\psi(\partial_\mu V_\nu - \partial_\nu V_\mu), \quad (26)$$

one obtains for the scattering operator ( $m_V$  is the mass of the vector meson)

$$\hat{T} = \frac{1}{t - m_V^2} \left\{ g^2 [-V] - gf \left[ V + \frac{u-s}{4m_N^2} S + \frac{t}{8m_N^2} T + \frac{u-s}{4m_N^2} P \right] - f^2 \left[ \frac{t}{8m_N^2} T + \frac{u-s}{4m_N^2} P \right] \right\}. \quad (27)$$

Obviously a characteristic factor  $u - s \sim \cos\vartheta$  occurs in front of the invariants  $S$  and  $P$  as well as a factor  $t$  in front of  $T$ . This structure is, for the case of  $\rho$  exchange, of decisive importance for a correct behavior of the  $NN$

interaction. However, since we have to apply approximations when evaluating the dispersion integral (by introducing a cutoff  $t_c = 4m_N^2$ ), this structure is not automatically obtained when doing a straightforward calculation. Therefore we decided to transform these factors directly into the  $NN$  channel and to apply the dispersion integral for the remaining part of the spectral functions. (In a more formal language, new invariant operators have to be defined which include these factors.) Trivially the results are then forced to have the structure of  $s$ -channel vector meson exchange.

Another important modification of the above formulas remains to be introduced. So far, by construction (see Fig. 4), our results contain not only the correlated part we are interested in, but also the uncorrelated contribution, cf. Fig. 1. Therefore the latter has to be removed. We do this by subtracting the Born term part of the  $^J N$  functions of Eq. (15), which leads to new functions  $^J N_{corr}$  given by

$$^J N_{corr}(00; 00) = -C[(t_{0+}^0)^\dagger t_{0+}^0 - (v_{0+}^0)^\dagger v_{0+}^0] \quad (28)$$

for the pion and analogous extensions for the other channels. These new functions  $^J N_{corr}$  are actually used when evaluating the spectral functions by means of Eq. (17).

We still have to transform the isospin part of the  $N\bar{N} \rightarrow N\bar{N}$  amplitude into the  $s$ -channel. Resulting isospin factors are provided by the isospin crossing matrix [15]. In general we have

$$\begin{aligned} f_{NN}^{I=0} &= \frac{1}{2}(f_{N\bar{N}}^{I=0} - 3f_{N\bar{N}}^{I=1}) \\ f_{NN}^{I=1} &= \frac{1}{2}(f_{N\bar{N}}^{I=0} + f_{N\bar{N}}^{I=1}) \end{aligned} \quad (29)$$

for the connection of isospin factors in both channels. The factors for our  $N\bar{N} \rightarrow N\bar{N}$  amplitude are already implicitly taken into account by including corresponding factors in  $v_{N\bar{N} \rightarrow \pi\rho}$  and  $T_{\pi\rho \rightarrow \pi\rho}$ . For the (isospin zero)  $\omega$  and  $H_1$  channels we thus have  $f_{N\bar{N}}^I = \delta_{I,0}$  whereas in  $\pi$  and  $A_1$  we have  $f_{N\bar{N}}^I = \delta_{I,1}$ . Therefore our final result for the correlated  $\pi\rho$  exchange  $NN$  potential can be written as operator in isospin space in the following way:

$$V_{\pi\rho,corr} = \frac{\kappa}{2} \sum_i \left[ \sum_{\alpha=\omega, H_1} \int_{(m_\pi+m_\rho)^2}^{t_c} dt' \frac{\rho_i^\alpha(t')}{t'-t} C_i \mathbf{1} + \sum_{\beta=\pi, A_1} \int_{(m_\pi+m_\rho)^2}^{t_c} dt' \frac{\rho_i^\beta(t')}{t'-t} C_i \tau_1 \cdot \tau_2 \right], \quad (30)$$

where  $C_i$ , according to the foregoing discussion, are matrix elements between nucleon helicity spinors of slightly modified invariants  $(u-s)S$ ,  $(u-s)P$ ,  $V$ ,  $A$ ,  $tT$ . The factor  $\kappa = \frac{1}{(2\pi)^3} \frac{m_N^2}{\sqrt{E_1 E_1' E_2 E_2'}}$  arises because  $V_{\pi\rho,corr}$  is to be defined as part of the Bonn potential whose  $T$ -matrix is defined by

$$S_{fi} = \delta_{fi} - i 2\pi \delta^{(4)}(p_1' + p_2' - p_1 - p_2) T_{fi}. \quad (31)$$

In order to be used in a scattering equation the resulting potential must be given off shell, as function of the in- and outgoing cm relative momenta and total energy in the  $s$  ( $NN$ ) channel, i.e.  $V = V(p', p; E_{cm})$ . On shell, for  $p' = p = p_0$  with  $E_{cm}^2 = 4(m_N^2 + p_0^2)$ , the relation of these variables to the Mandelstam variables is unique and given by

$$\begin{aligned} s &= 4E(p)^2 \\ t &= -2p^2(1 - \cos \vartheta) \\ u &= -2p^2(1 + \cos \vartheta). \end{aligned} \quad (32)$$

Half-off-shell, i.e. for  $p' \neq p$ , we take the plausible prescription  $t = -(\mathbf{p} - \mathbf{p}')^2$  and  $s = 4E(p)E(p')$ , which of course agrees with Eq. (32) on shell. Dependence on the starting energy is assumed to be of the same type as in time-ordered perturbation theory applied in the Bonn potential. Here the propagator of an exchanged meson reads

$$\frac{1}{\omega(E_{cm} - E(p) - E(p') - \omega)}. \quad (33)$$

In order to obtain a natural generalization of this expression we first define the 'on-mass-shell energy of an exchanged  $\pi\rho$  system',  $\Omega \equiv \sqrt{t' + (\mathbf{p} - \mathbf{p}')^2} = \sqrt{t' - t}$  and replace the energy denominator of the dispersion integral by the on-shell-equivalent expression

$$\frac{1}{t' - t} \rightarrow \frac{1}{\Omega(E_{cm} - E(p) - E(p') - \Omega)}. \quad (34)$$

Finally the resulting potentials have to fall off sufficiently rapidly in order to be able to solve the scattering equation. For this reason we introduce an additional form factor,  $\left(\frac{n\Lambda^2 - m^2}{n\Lambda^2 - t}\right)^n \rightarrow \left(\frac{n\Lambda^2 - t'}{n\Lambda^2 - t}\right)^n$ , with  $\Lambda = 5$  GeV,  $n=5$ , into the dispersion integral. The large cutoff mass chosen ensures that the results are not modified on shell.

## E. Determination of effective coupling constants and masses

It is convenient to parametrize our correlated  $\pi\rho$  exchange results in terms of single, sharp-mass effective meson exchange, as done for the analogous case of correlated  $\pi\pi$  in the  $NN$  [11] and  $\pi N$  [16] system. For reasons to be discussed below, this can only be done successfully for the  $\pi$  and  $\omega$  channel contributions. For an effective  $\pi'$  the scattering operator reads

$$\hat{T} = -g_{\pi'NN}^2 \vec{\tau}_1 \vec{\tau}_2 \frac{1}{t - m_{\pi'}^2} P \quad (35)$$

For the  $\omega'$ , the expression has already been given in Eq. (27). By comparison of the coefficients belonging to the invariants with the corresponding dispersion-theoretic terms one can determine an effective coupling constant, which will in general be  $t$ -dependent. For example we have for the pionic channel

$$-g_{\pi'NN}^2(t) \frac{1}{t - m_{\pi'}^2} = \frac{1}{2} \left[ \frac{1}{\pi} \int_{(m_\pi + m_\rho)^2}^{\infty} \frac{\rho_P^\pi(t')}{t' - t} dt' \right], \quad (36)$$

The effective mass  $m_{\pi'}$  is chosen such that  $g_{\pi'NN}$  becomes essentially independent of  $t$ . It turns out that for the  $H_1$  channel such a mass cannot be found. For channels involving several invariants, different coupling constants (and masses) are obtained which depend on the specific invariant for which the comparison is made. Obviously such a parametrization is successful if the resulting values only weakly (if at all) depend on the invariant chosen. This is the case for the  $\omega$ -channel but not for the  $A_1$ -channel.

## III. RESULTS AND DISCUSSION

Having introduced the necessary formalism for the evaluation of correlated  $\pi\rho$  exchange we now present the results and investigate their consequences for the  $NN$  interaction. We start with the results obtained in the  $t$ -channel, i.e. for the  $N\bar{N} \rightarrow \pi\rho$  amplitude and the spectral functions. We then discuss the properties of the resulting potential contribution, which is obtained from the (dispersion-theoretic) transformation into the  $s$ -channel, and point out its role within the Bonn meson exchange  $NN$  interaction [2].

### A. The $\pi$ channel

The pionic channel of correlated  $\pi\rho$  exchange is of special importance. As mentioned in the introduction it is a natural candidate to provide additional (short ranged) tensor force required to fit empirical  $NN$  data with models using a realistic, soft  $\pi NN$  form factor.

Fig. 8 shows the  $N\bar{N} \rightarrow \pi\rho$  (on-shell) potential  $v_{N\bar{N} \rightarrow \pi\rho}$  and the corresponding amplitude  $t_{N\bar{N} \rightarrow \pi\rho}$  obtained from Eq. (17), which contains the effect of  $\pi\rho$  correlations. The purely imaginary potential has a strong increase at the pseudophysical  $\pi\rho$  threshold and a maximum near  $t = 50m_\pi^2$ .  $\pi\rho$  correlations strengthen this maximum; in addition they generate a real part in the amplitude. Note that these modifications act quadratically in the  $NN \rightarrow NN$  amplitude and therefore also in the  $NN$  potential, so that the final effect of  $\pi\rho$  correlations is stronger than Fig. 8 suggests.

Indeed, the spectral function  $\rho_P^\pi(t)$  in Fig. 9 demonstrates that the piece due to correlated  $\pi\rho$  exchange has a considerable strength, although it is smaller than the uncorrelated part generated by the transition potential only. One has to keep in mind that a good part of the latter contribution consists of iterative  $\pi\rho$  box diagrams involving  $NN$  intermediate states, which are not part of  $V_{NN}$  but are generated by the  $NN$  scattering equation. Consequently the role of uncorrelated processes in  $V_{NN}$  is considerably smaller than suggested from the figure.

The spectral function of the correlated part has a clear maximum at about  $t=60 m_\pi^2$ , thus representing the mass distribution of a broad, heavy effective particle with pionic quantum numbers. A rough parametrization of this contribution by sharp-mass particle exchange appears to require a mass of about 1 GeV, noticeably smaller than chosen in Ref. [17] for the phenomenological  $\pi'$ .

In the  $s$ -channel we first demonstrate the influence of the resulting on-shell potentials in the  ${}^3S_1 - {}^3D_1$  and  ${}^1S_0$  partial waves as function of the nucleon lab energy. In Fig. 10 the dotted and dashed curves show the corresponding one-pion-exchange (OPE) potentials; obviously there is a strong suppression of OPEP when the  $\pi NN$  cutoff mass



is reduced from the value of 1.3 GeV used in the full Bonn potential to 1 GeV. Most importantly, the addition of the potential due to correlated  $\pi\rho$  exchange in the pionic channel to the dotted curve restores the original tensor force strength; obviously it is able to counterbalance the suppression induced by the smaller  $\pi NN$  cutoff mass. The  ${}^3S_1 - {}^3D_1$  partial wave is of special importance in this connection since it exclusively contains a tensor force component, which is decisive for a realistic description of deuteron properties.

It should be added that the above result is in remarkable agreement with a previous calculation of the  $\pi NN$  form factor [3], Fig. 11, which consistently used the same  $\pi\rho$   $t$ -matrix and  $N\bar{N} \rightarrow \pi\rho$  transition potential, and independently arrived at  $\Lambda_{\pi NN} = 1$  GeV.

As discussed in Sect. IIE, correlated  $\pi\rho$  exchange in the  $\pi$  and  $\omega$  channels can be parametrized by sharp-mass one-boson-exchange (OBE) potentials, provided that the effective coupling constants are allowed to become  $t$ -dependent. Fig. 12 shows such coupling constants for the exchange of a heavy  $\pi'$  for various chosen masses of  $\pi'$ . Obviously the coupling becomes  $t$ -independent for a mass of 1020 MeV, quite near the maximum of the correlated spectral function in Fig. 9, and the resulting coupling constant is  $g_{\pi' NN}^2/4\pi \simeq 9$ . If we choose  $m_{\pi'} = 1200$  MeV as in [17], the resulting coupling constant is noticeably  $t$ -dependent; its strength is much smaller than used in [17]. There are two reasons for this discrepancy: First the authors of [17] applied a  $\pi' NN$  form factor, which reduces the strength at  $t=0$  (relevant for  $NN$  scattering) by more than a factor of 2. Second, the strength of the  $\pi'$  was phenomenologically chosen in [17] to compensate for a much softer  $\pi NN$  form factor, with a cutoff mass of 800 MeV. (Indeed a much smaller value ( $g_{\pi' NN}^2/4\pi = 70$ ) is sufficient to compensate for a form factor with  $\Lambda_{\pi NN} = 900$  MeV [18].) Obviously correlated  $\pi\rho$  exchange can only partly explain the phenomenological  $\pi'$ ; another possible mechanism is correlated  $\pi\sigma$  exchange [19] (where  $\sigma$  stands for correlated  $\pi\pi$  exchange in the S-wave channel).

In order to show that the compensation for a softer  $\pi NN$  form factor by correlated  $\pi\rho$  exchange is valid not only for on-shell potentials, but also for  $NN$  amplitudes and observables, we extrapolate the correlated  $\pi\rho$  exchange off shell as described in Sect. IID, add this piece to the (full) Bonn potential (with a reduced  $\pi NN$  cutoff mass of 1 GeV) and solve the relativistic Schroedinger equation relevant for the Bonn potential. Only a slight readjustment of the coupling of the isospin-one scalar meson ( $\delta$  in [2]) in the original Bonn potential is required in order to obtain again a good description of  $NN$  phase shifts.

As Table IV demonstrates convincingly the deuteron observables also can be reproduced with a considerably softer  $\pi NN$  form factor (characterized by  $\Lambda_{\pi NN} = 1$  GeV), provided that correlated  $\pi\rho$  exchange in the pionic channel is included.

## B. The $\omega$ -channel

Since the mass of the physical  $\omega$ -meson is only slightly below the  $\pi\rho$  threshold, genuine pole terms have been included in the  $\pi\rho$  amplitude [10] as well as in our model for the transition potential  $v_{N\bar{N} \rightarrow \pi\rho}$ . As Fig. 13(a) shows, the contribution of such pole terms leads to a reduction of the (imaginary) transition potential above the  $\pi\rho$  threshold, whose amount depends on the value of the bare coupling constant  $g_{\omega NN}^{(0)}$ . (The reason for our choice  $g_{\omega NN}^{(0)}/4\pi = 4.40$  will be discussed later.) Fig. 13(b) shows the resulting amplitude  $t_{N\bar{N} \rightarrow \pi\rho}$ . Similarly to the pionic channel,  $\pi\rho$  correlations enhance the maximum of the amplitude near threshold.

The inclusion of the  $\omega$ -meson pole terms in our dynamical model ensures that the imaginary part of the  $N\bar{N} \rightarrow N\bar{N}$  amplitude, and therefore the resulting  $NN$  potential, contains, besides ‘true’ correlated  $\pi\rho$  exchange (Fig. 14(e)) generated by the non-pole parts of the corresponding amplitudes, also genuine  $\omega$  exchange processes (Fig. 14(a)-(d)). Corresponding propagators and vertex functions are dressed by  $\pi\rho$  loop corrections. For example, the  $\omega$  propagator has the following structure (for details we refer the reader to [10]):

$$d = \frac{1}{t - (m_\omega^{(0)})^2 - \Sigma(t)}, \quad \text{with} \quad \Sigma(t) \sim \int f^{(0)} G_{\pi\rho} f, \quad (37)$$

where  $f^{(0)}$  and  $f$  are bare and dressed  $\omega \rightarrow \pi\rho$  vertex functions, respectively, and  $G_{\pi\rho}$  denotes the  $\pi\rho$  propagator.

The bare parameters  $g_{\omega\pi\rho}^{(0)}$  and  $m_\omega^{(0)}$  have been adjusted such that  $d$  has a pole at  $t = m_\omega^2$ . The imaginary part of the  $N\bar{N} \rightarrow N\bar{N}$  amplitude, and therefore the corresponding spectral functions, consist of a  $\delta$ -function at  $t = m_\omega^2$ , which precisely corresponds to the exchange of a (physical)  $\omega$ -meson with point-like  $\omega NN$  coupling, i.e. without any form factor. However it is important to realize that  $d$ , and therefore the diagrams in Fig. 14(a)-(d), provide a further contribution, since  $\pi\rho$  intermediate states make the self-energy  $\Sigma$  complex above the  $\pi\rho$  threshold. Such intermediate states likewise occur at the vertices in diagrams (b)-(d), leading to additional contributions to the spectral functions.

Fig. 15 shows the resulting spectral functions. Note that although we assumed the bare  $\omega NN$  coupling to be of pure vector type, small contributions to  $\rho_S$ ,  $\rho_T$ , and  $\rho_P$  occur, which are generated by the  $\pi\rho$  loops in Fig. 14(b)-(d). First

we have the  $\delta$ -function piece (dashed); above  $\pi\rho$  threshold we have additional contributions from diagrams 14(a)-(d) (dash-dotted) which have opposite sign to the  $\delta$ -function. They act as vertex corrections which suppress the point-like coupling of  $\omega$  exchange and thus generate a form factor effect. Finally there is a sizable non-pole contribution (dotted curve); throughout it has opposite sign to the part generated by the vertex corrections and roughly counterbalances their effect, a fact found already in the pionic channel.

Again, after presenting the results in the  $t$ -channel, we now want to look at the corresponding on-shell potentials in the  $s$ -channel. Since we deal with rather short-ranged contributions we show, as two characteristic examples, the results for the  $^1S_0$  and  $^3P_1$  partial waves (Fig. 16). Note that the bare  $\omega NN$  coupling ( $g_{\omega NN}^{(0)}=4.40$ ), which determines the size of diagrams (a)-(c), has been chosen such that the total repulsion generated by all diagrams of Fig. 14 agrees (at low energies) with the effective  $\omega$  exchange in the Bonn potential needed empirically. The dashed curves are generated by the  $\delta$ -functions in Fig. 15, with a predicted renormalized coupling constant of  $g_{\omega NN}^2=11.0$ . Apparently this contribution alone provides almost the same repulsion as in the Bonn potential although the coupling constant is about a factor of 2 smaller. The reason is that the phenomenological form factor in the Bonn potential, with the monopole cutoff mass (1.5 GeV) of only twice the  $\omega$  mass, leads to a strong reduction of the coupling constant in the physical region ( $g_{\omega NN}^2(t=0)=10.6$ ). The vertex corrections (generated by diagrams (a)-(d) above  $\pi\rho$  threshold) strongly reduce the repulsion in the physical region, leading to the dash-dotted curve. This suppression is essentially cancelled by the ‘true’ correlated  $\pi\rho$  exchange (diagram 14 (e)), as already demonstrated for the spectral functions. Obviously the latter contribution is remarkably strong; it explains about 40% of effective  $\omega$  exchange.

The new reduced coupling constant (11.0) is still about a factor of 2 larger than provided by customary SU(3) estimates, which use  $g_{\omega NN}^2=9g_{\rho NN}^2$ . Thus with  $g_{\rho NN}^2/4\pi=0.55$  as determined by Hoehler and Pietarinen [20] we have  $g_{\omega NN}^2/4\pi \simeq 5$ . Note however that the above relation between  $\omega$  and  $\rho$  coupling constants is based, apart from ideal mixing, on the assumption of vanishing  $\phi NN$  coupling. For  $g_{\phi NN}$  unequal to zero the above relation goes into

$$g_{NN\omega} = 3g_{NN\rho} - \sqrt{2}g_{NN\phi} . \quad (38)$$

Thus if we take  $g_{\phi NN} = -g_{\rho NN}$  (which amounts to a rather small deviation from zero) we have  $g_{\omega NN}^2 \approx 20g_{\rho NN}^2$ , in rough agreement with our results. Such a value for the  $\phi NN$  coupling to the nucleon and the negative sign is well conceivable, if the  $\phi$  couples to the nucleon via the  $K\bar{K}$  continuum [21].

As discussed before, for practical reasons it is convenient to parametrize also the non-pole contribution of diagram 14(e) by an effective one-boson-exchange. Results are shown in Fig. 17, for the dominant vector as well as the tensor coupling. Obviously they can be reasonably represented by  $g_{\omega' NN}^2/4\pi=8.5$ ,  $f_{\omega' NN}/g_{\omega' NN}=0.4$ , and  $m_{\omega'}=1120$  MeV. Using the mass of the physical  $\omega$  meson  $m_\omega = 782$  MeV we find a ( $t$ -dependent) effective  $\omega$  coupling strength characterized by  $g_{\omega NN}^2 \simeq 4$ . It is interesting to note that the suppression of the tensor coupling, in some sense enforced in the pole terms by assuming the corresponding bare coupling to be zero, also happens in the non-pole term.

### C. The $A_1/H_1$ -channel

After the discussion of the  $\pi$  and  $\omega$  channel we now want to investigate the  $A_1$  and  $H_1$  channels together since their structure is very similar. Compared to the  $\pi$  and  $\omega$  channels we have important differences. First the  $A_1$  as well as the  $H_1$  mass lie above the  $\pi\rho$  threshold, and both particles decay with a very large width into  $\pi\rho$ . Consequently their propagators now acquire a pole in the complex plane. Second, in contrast to the  $\pi$  and  $\omega$  channels, the Bonn potential [2] does not contain  $A_1/H_1$  OBE contributions, which could be used to fix the bare  $A_1 NN$  and  $H_1 NN$  coupling constants, as was done in the  $\omega$  channel. Since there is no other *a priori* information about these couplings, we will in this first extrapolatory study, simply put them to zero, i.e. take only diagrams of type 14(d) and (e) into account. If, in a later stage, those couplings turn out to be needed (e.g. in order to obtain a quantitative fit to the  $NN$  data), they should be included.

There is a further structural difference which has an enormous impact on the results and requires an extended discussion. In general, besides the unitarity cut for  $t > (m_\pi + m_\rho)^2$  treated in the dispersion integral (Eq. (8)), there exists a left hand cut for  $t < t_0$  in the  $N\bar{N} \rightarrow \pi\rho$  amplitude generated by  $s$ -channel poles due to nucleon and  $\Delta$ -isobar exchange (Fig. 5).  $t_0$  is fixed by the condition  $s - m_{N/\Delta}^2 = 0$ . There are two solutions for each exchange; the largest value (generated by nucleon exchange) is at  $t_0 \approx 42m_\pi^2$ , i.e. just below the  $\pi\rho$  threshold. Consequently this branch point will influence the resulting potentials near threshold considerably.

In the  $\pi$  and  $\omega$  channels the corresponding potentials act in P-waves and are thus proportional to the  $\pi\rho$  on-shell momentum  $k_0$ , with the effect that the corresponding transition potentials start to increase first when approaching the threshold, but are then suppressed by the  $k_0$  factor. In this way one obtains the characteristic structure of a maximum near threshold, which we have observed in such channels. The point now is that both the  $A_1$  and  $H_1$  are

$\pi\rho$  S-waves; therefore the transition potentials do not contain the damping factor  $k_0$  anymore. Indeed, Figs. 18 and 19 show the overwhelming effect of the left hand cut near threshold, in both channels. It essentially remains when  $\pi\rho$  correlations (which contain the  $A_1$  resonance) are included, although the influence of the  $A_1$  is clearly seen.

Fig. 20 shows the resulting spectral functions  $\rho_P^{H_1}$ ,  $\rho_A^{A_1}$ , and  $\rho_P^{A_1}$ . Again the strong effect of the left hand cut near threshold is obvious. Note also that for  $\rho_P$ ,  $A_1$  and  $H_1$  provide roughly similar contributions, but with opposite sign.

In Fig. 21 we present the resulting on-shell potentials in some selected partial waves. For both S-states, the (attractive)  $A_1$  contribution strongly dominates the result arising from the  $H_1$  channel but is considerably smaller (as far as the modulus is concerned) compared to the corresponding piece in the  $\omega$  channel, cf. Fig. 17. For  ${}^3P_1$  both contributions have opposite sign and roughly cancel; the total result is negligible compared to the  $\omega$  channel.

In contrast to the  $\pi$ ,  $\omega$  channels discussed before, the above results cannot be suitably parametrized in terms of sharp-mass exchanges. In case of the  $A_1$ , no reasonable mass can be found which works for both spectral functions; moreover all effective coupling constants become strongly  $t$ -dependent. The basic reason is again the dominance of the left hand cut, which destroys the conventional bump structure of the spectral functions found in other channels of correlated  $\pi\pi$  and  $\pi\rho$  exchange.

#### IV. CONCLUDING REMARKS

In this work we have determined the contribution to the  $NN$  interaction due to the exchange of a correlated  $\pi\rho$  pair between two nucleons. The correlations between  $\pi$  and  $\rho$  have been taken into account using a realistic meson exchange model of the  $\pi\rho$  interaction [10]. In a first step we evaluated the  $t$ -channel amplitude  $N\bar{N} \rightarrow N\bar{N}$  including  $\pi\rho$  correlations. The transformation into the  $s$ -channel with the help of dispersion-theoretic methods then yields the correlated  $\pi\rho$  exchange  $NN$  potential. We have investigated four relevant channels of the  $\pi\rho$  system characterized by the quantum numbers of the physical particles  $\pi$ ,  $\omega$ ,  $A_1$ , and  $H_1$ .

In the pionic channel correlated  $\pi\rho$  exchange yields a short-ranged contribution, which roughly corresponds to an exchange of a heavy (effective)  $\pi'$  with a mass of about 1 GeV. The additional tensor force generated by this potential is sufficient to compensate for a reduction of the  $\pi NN$  cutoff mass  $\Lambda_{\pi NN}$  from 1.3 GeV to 1.0 GeV in the one-pion-exchange potential. For basic theoretical reasons, such a reduction is highly welcome, since various models of nucleon structure unanimously predict a rather soft  $\pi NN$  form factor characterized by  $\Lambda_{\pi NN} \simeq 0.8$  GeV. Such a small value might be reached if correlated  $\pi\sigma$  exchange is included, too, which is also missing in the Bonn potential. (As usual,  $\sigma$  stands for a low mass correlated  $\pi\pi$  pair in the  $0^+$  channel.) Thus it appears that in the Bonn potential [2] the one-pion-exchange potential together with a hard form factor is an effective description of ‘true’ one-pion exchange (with a soft form factor) plus correlated  $\pi\rho$  (and  $\pi\sigma$ ) exchange in the pionic channel.

In the  $\omega$  channel, the exchange of a correlated  $\pi\rho$  pair also provides a sizable contribution to the  $NN$  interaction. Since the  $\omega$  mass is near the  $\pi\rho$  threshold we have included the genuine  $\omega$ -meson explicitly and replaced the (effective)  $\omega$  exchange in the Bonn potential by the resulting correlated  $\pi\rho$  potential, which can be decomposed into a pole and a non-pole piece. The former provides a microscopic model for ‘true’  $\omega$  exchange leading to a renormalized  $\omega NN$  coupling constant,  $g_{\omega NN}^2/4\pi = 11.0$ , which is about a factor of two smaller than the effective value of 20 used in the Bonn potential. Thus ‘true’ correlated  $\pi\rho$  exchange (Fig. 1(e)) provides almost half of the empirical repulsion needed in the  $NN$  interaction; it can be parametrized by sharp-mass  $\omega'$  exchange with  $g_{\omega' NN}^2 \simeq 8.5$ ,  $f_{\omega' NN}/g_{\omega' NN} \simeq 0.4$  and  $m_{\omega'} \simeq 1120$  MeV.

Our present result for the  $\omega$  coupling constant ( $g_{\omega NN}^2 \approx 20g_{\rho NN}^2$ ) is well compatible with  $SU(3)$ , provided that there exists a small, negative  $\phi NN$  coupling of vector type, with the magnitude of the order of the  $\rho$ -coupling. Such a  $\phi NN$  coupling (especially the required negative sign) occurs naturally if it is supposed to arise via the  $K\bar{K}$  continuum. Although corresponding  $\phi$  exchange in the  $NN$  interaction provides only a small contribution to the repulsion, it makes the above relation between  $\omega$  and  $\rho$  couplings agree with  $SU(3)$  predictions. Consequently there appears to be little room for explicit quark-gluon effects in being responsible for the short-range  $NN$  repulsion.

Additional contributions arise in the  $A_1$  and  $H_1$  channels. They are sizable individually, mainly due to left-hand cut effects arising from nucleon and  $\Delta$  exchange in a  $\pi\rho$  S-wave. However, in some partial waves strong cancellations occur between the  $A_1$  and  $H_1$  contributions. Further contributions are, in principle, generated by direct coupling of the  $A_1/H_1$  to the nucleon. The size of such couplings is, however, not known; these terms are therefore omitted in the present work. It remains to be seen whether a precise fit of the  $NN$  observables requires such terms and thereby establishes their existence.

## APPENDIX A: DETERMINATION OF SPECTRAL FUNCTIONS

In this appendix we derive Eq. (17) of the main text, which provides the connection between the spectral functions needed in Eq. (8) and the imaginary part of the  $N\bar{N} \rightarrow N\bar{N}$  amplitude in the LSJ basis ( $^J N$ ) obtained from the unitarity relation (Eq. (9)). For the latter it was necessary to work in the LSJ basis in order to identify the allowed  $N\bar{N} \rightarrow \pi\rho$  transitions. In order to establish the connection to the spectral functions however, matrix elements of the invariants  $\hat{C}_j$  are required, which is most suitably done in the helicity state basis. The imaginary part of the  $N\bar{N} \rightarrow N\bar{N}$  amplitude is now defined by (cf. Eq. (12) for the analogous definition in LSJ basis)  $^J N(\lambda'_N \lambda'_{\bar{N}}; \lambda_N \lambda_{\bar{N}}) \equiv \text{Im} T^J(p' \lambda'_N \lambda'_{\bar{N}}; p \lambda_N \lambda_{\bar{N}}; \sqrt{t})$  and the relation between LSJ and helicity basis amplitudes is given by the standard expressions (cf. [2])

$$\begin{aligned}
^J N_1 &= \frac{1}{2} ^J N(J0; J0) + a^2 ^J N(J-11; J-11) - ab ^J N(J+11; J-11) \\
&\quad - ab ^J N(J-11; J+11) + b^2 ^J N(J+11; J+11) \\
^J N_2 &= -\frac{1}{2} ^J N(J0; J0) + a^2 ^J N(J-11; J-11) - ab ^J N(J+11; J-11) \\
&\quad - ab ^J N(J-11; J+11) + b^2 ^J N(J+11; J+11) \\
^J N_3 &= \frac{1}{2} ^J N(J1; J1) + b^2 ^J N(J-11; J-11) + ab ^J N(J+11; J-11) \\
&\quad + ab ^J N(J-11; J+11) + a^2 ^J N(J+11; J+11) \\
^J N_4 &= -\frac{1}{2} ^J N(J1; J1) + b^2 ^J N(J-11; J-11) + ab ^J N(J+11; J-11) \\
&\quad + ab ^J N(J-11; J+11) + a^2 ^J N(J+11; J+11) \\
^J N_5 &= ab ^J N(J-11; J-11) - b^2 ^J N(J+11; J-11) + a^2 ^J N(J-11; J+11) \\
&\quad - ab ^J N(J+11; J+11) \\
^J N_6 &= ^J N_5 \quad (\text{on-shell})
\end{aligned} \tag{A1}$$

where we used the short-hand notation for the  $^J N$  amplitudes defined in Table V and

$$a = \sqrt{\frac{J}{2(2J+1)}} \quad b = \sqrt{\frac{J+1}{2(2J+1)}} \tag{A2}$$

The various channel contributions to  $\text{Im} T(\mathbf{p}' \lambda'_N \lambda'_{\bar{N}}; \mathbf{p} \lambda_N \lambda_{\bar{N}}; \sqrt{t})$  are then given by

$$\begin{aligned}
\pi : N_i &\equiv N(\lambda'_N \lambda'_{\bar{N}}; \lambda_N \lambda_{\bar{N}}) \equiv \frac{1}{4\pi} d_{\lambda\lambda'}^0(\cos\vartheta) {}^0 N(\lambda'_N \lambda'_{\bar{N}}; \lambda_N \lambda_{\bar{N}}) \equiv \frac{1}{4\pi} d_{\lambda\lambda'}^0(\cos\vartheta) {}^0 N_i \\
\omega, A_1, H_1 : N_i &\equiv N(\lambda'_N \lambda'_{\bar{N}}; \lambda_N \lambda_{\bar{N}}) \equiv \frac{3}{4\pi} d_{\lambda\lambda'}^1(\cos\vartheta) {}^1 N(\lambda'_N \lambda'_{\bar{N}}; \lambda_N \lambda_{\bar{N}}) \equiv \frac{3}{4\pi} d_{\lambda\lambda'}^1(\cos\vartheta) {}^1 N_i
\end{aligned} \tag{A3}$$

We now define a vector  $\mathbf{N}^\alpha = (N_1^\alpha \ N_2^\alpha \ N_3^\alpha \ N_4^\alpha \ N_5^\alpha)$ ,  $\alpha = \pi, \omega, A_1, H_1$ , and use Eqs. (15) and (A1) to express its components in terms of the LSJ amplitudes  $^J N(L'S'; LS)$  for each of the contributing channels. We obtain

$$\mathbf{N}^\pi = \begin{pmatrix} \frac{1}{8\pi} {}^0 N(00; 00) \\ -\frac{1}{8\pi} {}^0 N(00; 00) \\ 0 \\ 0 \\ 0 \end{pmatrix}, \tag{A4}$$

$$\mathbf{N}^{A_1} = \begin{pmatrix} 0 \\ 0 \\ \frac{3(1+\cos\vartheta)}{16\pi} {}^1 N(11; 11) \\ \frac{3(-1+\cos\vartheta)}{16\pi} {}^1 N(11; 11) \\ 0 \end{pmatrix}, \tag{A5}$$

$$\mathbf{N}^{H_1} = \begin{pmatrix} \frac{3 \cos \vartheta}{8\pi} {}^1N(00; 00) \\ -\frac{3 \cos \vartheta}{8\pi} {}^1N(00; 00) \\ 0 \\ 0 \\ 0 \end{pmatrix}, \quad (\text{A6})$$

$$\mathbf{N}^\omega = \begin{pmatrix} \frac{3}{4\pi} \cos \vartheta [\frac{1}{6} {}^1N(01; 01) - \sqrt{\frac{2}{9}} {}^1N(01; 21) + \frac{1}{3} {}^1N(21; 21)] \\ \frac{3}{4\pi} [\frac{1}{6} {}^1N(01; 01) - \sqrt{\frac{2}{9}} {}^1N(01; 21) + \frac{1}{3} {}^1N(21; 21)] \\ \frac{1}{16\pi} (1 + \cos \vartheta) [2 {}^1N(01; 01) + 2\sqrt{2} {}^1N(01; 21) + {}^1N(21; 21)] \\ -\frac{1}{16\pi} (-1 + \cos \vartheta) [2 {}^1N(01; 01) + 2\sqrt{2} {}^1N(01; 21) + {}^1N(21; 21)] \\ \frac{1}{16\pi} \sin \vartheta [-2 {}^1N(01; 01) + \sqrt{2} {}^1N(01; 21) + 2 {}^1N(21; 21)] \end{pmatrix}. \quad (\text{A7})$$

The decomposition of the imaginary part of Eq. (4) can now be written for the helicity state matrix-elements in matrix notation

$$\mathbf{N}^{\pi, \omega, A_1, H_1} = \begin{pmatrix} S_1 & V_1 & T_1 & P_1 & A_1 \\ S_2 & V_2 & T_2 & P_2 & A_2 \\ S_3 & V_3 & T_3 & P_3 & A_3 \\ S_4 & V_4 & T_4 & P_4 & A_4 \\ S_5 & V_5 & T_5 & P_5 & A_5 \end{pmatrix} \mathbf{R} \equiv \mathbf{M} \mathbf{R} \quad (\text{A8})$$

where  $\mathbf{R} = (\rho_S \rho_V \rho_T \rho_P \rho_A)$ .  $S_i, V_i, T_i, P_i,$  and  $A_i$  are helicity state matrix-elements of the Fermi invariants using the same indexing as for the  $N$  amplitudes and we find

$$\mathbf{M} = \begin{pmatrix} \beta^2 - 1 & -\cos \vartheta & -2 \cos \vartheta & -\beta^2 & 1 \\ \beta^2 - 1 & -\cos \vartheta & 2 \cos \vartheta (-2\beta^2 + 1) & \beta^2 & -1 \\ 0 & -\beta^2 (1 + \cos \vartheta) & -2(1 + \cos \vartheta) & 0 & -(\beta^2 - 1)(1 + \cos \vartheta) \\ 0 & -\beta^2 (1 - \cos \vartheta) & -2(1 - \cos \vartheta) & 0 & (\beta^2 - 1)(1 - \cos \vartheta) \\ 0 & \beta \sin \vartheta & 2\beta \sin \vartheta & 0 & 0 \end{pmatrix} \quad (\text{A9})$$

The spectral functions are then simply obtained by calculating  $\mathbf{R} = \mathbf{M}^{-1} \mathbf{N}^{\pi, \omega, A_1, H_1}$  yielding the result of Eq. (17).

- [1] G. Janssen, B.C. Pearce, K. Holinde, and J. Speth, Phys. Rev. D (in print).
- [2] R. Machleidt, K. Holinde, and Ch. Elster, Phys. Rep. **149**, 1 (1987).
- [3] G. Janssen, K. Holinde, and J. Speth, Phys. Rev. Lett. **73**, 1332 (1994).
- [4] T.E.O. Ericson and M. Rosa-Clot, Nucl. Phys. **A405**, 497 (1983).
- [5] T.E.O. Ericson and M. Rosa-Clot, Ann. Rev. Nucl. Part. Sci. **35**, 271 (1985).
- [6] K.F. Liu, S.J. Dong, T. Draper, and W. Wilcox, Phys. Rev. Lett. **74**, 2172 (1995).
- [7] S.A. Coon and M.D. Scadron, Phys. Rev. C **23**, 1150 (1981).
- [8] S.A. Coon and M.D. Scadron, Phys. Rev. D **42**, 2256 (1990).
- [9] A.W. Thomas and K. Holinde, Phys. Rev. Lett. **63**, 2025 (1989).
- [10] G. Janssen, K. Holinde, and J. Speth, Phys. Rev. C **49**, 2763 (1994).
- [11] H.-C. Kim, J.W. Durso, and K. Holinde, Phys. Rev. C **49**, 2355 (1994).
- [12] R. Blankenbecler and R. Sugar, Phys. Rev. **142**, 1051 (1966).
- [13] V. Mull, J. Haidenbauer, T. Hippchen, and K. Holinde, Phys. Rev. C **44**, 1337 (1991).
- [14] R. Aaron, *Modern Three-Hadron Physics* (Springer Verlag, Heidelberg, 1976).
- [15] A.D. Martin and T.D. Spearman, *Elementary Particle Theory* (North-Holland, Amsterdam, 1970).
- [16] C. Schütz, J.W. Durso, K. Holinde, and J. Speth, Phys. Rev. C **49**, 2671 (1994).
- [17] K. Holinde and A.W. Thomas, Phys. Rev. C **42**, R1195 (1990).
- [18] J. Haidenbauer, K. Holinde, and A.W. Thomas, Phys. Rev. C **49**, 2331 (1994).
- [19] T. Ueda, Phys. Rev. Lett. **68**, 142 (1992).
- [20] G. Hoehler and E. Pietarinen, Nucl. Phys. **B95**, 210 (1975).
- [21] V. Mull, private communication.

[22] J. A. Dankowych *et al.*, Phys. Rev. Lett. **38**, 580 (1981).

FIG. 1.  $\pi\rho$  contributions to the  $NN$  potential. (a) is generated by the scattering equation whereas (b) and (c) are explicitly contained in the Bonn potential. (d) shows correlated  $\pi\rho$  exchange treated in the present work.

FIG. 2. Diagram visualizing the  $NN$  scattering process, in the  $s$  ( $NN \rightarrow NN$ ) and  $t$  ( $N\bar{N} \rightarrow N\bar{N}$ ) channels.

FIG. 3. Diagram visualizing the  $\pi\rho$  exchange contribution to the  $NN$  interaction.

FIG. 4. The transition amplitude  $t_{N\bar{N} \rightarrow \pi\rho}$ .

FIG. 5. The transition potential  $v_{N\bar{N} \rightarrow \pi\rho}$ .

FIG. 6. Contributions to the  $\pi\rho$  potential.

FIG. 7. Results of our  $\pi\rho$  interaction model for the mass distribution in the  $H_1$  and  $A_1$  channels compared with experiment [22].

FIG. 8. The (imaginary) transition potential  $v_{N\bar{N} \rightarrow \pi\rho}$  (dashed curve) in the pion channel together with the corresponding amplitude  $t_{N\bar{N} \rightarrow \pi\rho}$ . The dotted line shows the real part of  $t$ , the solid line the imaginary part.

FIG. 9. The spectral function in the pionic channel  $\rho_P^\pi(t)$ . The dotted line shows the uncorrelated part whereas the solid line represents the correlated contribution.

FIG. 10. On-shell  $NN$  potential  $V_{NN}$  as function of the nucleon lab energy in the  $^1S_0$  state (a) and  $^3D_1 - ^3S_1$  transition (b). The dotted line denotes the one-pion-exchange potential as used in the Bonn potential ( $g_{\pi NN}^2/4\pi = 14.4$ ,  $\Lambda_{\pi NN} = 1.3$  GeV). For the dashed line,  $\Lambda_{\pi NN} = 1.0$  GeV. The solid line results if correlated  $\pi\rho$  exchange in the pionic channel is added to the dashed line.

FIG. 11. Diagrams contributing to the  $\pi NN$  form factor.

FIG. 12. The  $t$ -dependent effective  $\pi'NN$  coupling constant for various values of  $m_{\pi'}$ .

FIG. 13. The (imaginary) transition potential  $v_{N\bar{N} \rightarrow \pi\rho}$  (dashed curve) in the  $\omega$  channel (a) together with the corresponding amplitude  $t_{N\bar{N} \rightarrow \pi\rho}$  (b). The dotted line shows the real part of  $t$ , the solid line the imaginary part.

FIG. 14. Contributions to the  $NN$  potential in the  $\omega$  channel.

FIG. 15. The spectral functions in the  $\omega$  channel. As explained in the text the dashed line contains only the  $\delta$ -function contribution of diagrams 14 (a)-(d) whereas the dash-dotted line shows the vertex and propagator corrections to the corresponding diagrams. The dotted line contains only the non-pole part (14 (e)) and the solid line shows the full result.

FIG. 16. On-shell  $NN$  potential  $V_{NN}$  as function of the nucleon lab energy in the  $^1S_0$  and  $^3P_1$  state. The long-dashed line shows the result of single  $\omega$  exchange as contained in the Bonn potential ( $g_{\omega NN}^2/4\pi=20; \Lambda_{\omega NN}=1500$  MeV). The dashed line contains only the  $\delta$ -function contribution of the diagrams of Figs. 14(a)-(d) (cf. text) from which the dash-dotted line is obtained by adding the vertex and propagator corrections contained in the corresponding diagrams. The full result is shown by the solid line and contains in addition the non-pole part (Fig. 14(e)).

FIG. 17. The  $t$ -dependent effective  $\omega'NN$  vector coupling constant  $g_{\omega' NN}^2/4\pi$  and the ratio  $f_{\omega' NN}/g_{\omega' NN}$  for  $m_{\omega'}=1120$  MeV (solid). The dashed line shows  $g_{\omega' NN}^2/4\pi$  when the physical  $\omega$  mass (782.6 MeV) is used.

FIG. 18. The (real) transition potential  $v_{N\bar{N}\rightarrow\pi\rho}$  (dashed curve) in the  $A_1$  channel together with the corresponding amplitude  $t_{N\bar{N}\rightarrow\pi\rho}$ . The dotted line shows the real part of  $t$ , the solid line the imaginary part.

FIG. 19. Same as Fig. 18 but for the  $H_1$  channel.

FIG. 20. The spectral functions in the  $A_1$  and  $H_1$  channel ((a): $\rho_P^{H_1}$ ; (b): $\rho_P^{A_1}$ ; (c): $\rho_A^{A_1}$ ). The dashed line shows the contribution of the pole part whereas the dotted line contains the non-pole part. The full result is given by the solid line.

FIG. 21. On-shell  $NN$  potential  $V_{NN}$  as function of the nucleon lab energy in the  $^1S_0$ ,  $^3S_1$ , and  $^3P_1$  states. The dash-dotted (dotted) line shows correlated  $\pi\rho$  exchange in the  $A_1$  ( $H_1$ ) channel.

TABLE I. Quantum numbers and possible transitions from the  $N\bar{N}$  to the  $\pi\rho$  system.

	$J^P$	$(I^G)$	$L_{\pi\rho}$	$S_{\pi\rho}$	$L_{N\bar{N}}$	$S_{N\bar{N}}$	$L_{N\bar{N}}S_{N\bar{N}} \rightarrow L_{\pi\rho}S_{\pi\rho}$	notation
$\pi$	$0^-$	$(1^-)$	1	1	0	0	J 0 $\rightarrow$ J+1 1	$t_{0+}^J$
$\omega$	$1^-$	$(0^-)$	1	1	0	1	J-1 1 $\rightarrow$ J 1	$t_{-1}^J$
			1	1	2	1	J+1 1 $\rightarrow$ J 1	$t_{+1}^J$
$A_1$	$1^+$	$(1^-)$	0	1	1	1	J 1 $\rightarrow$ J-1 1	$t_{1-}^J$
			2	1	1	1	J 1 $\rightarrow$ J+1 1	$t_{1+}^J$
$H_1$	$1^+$	$(0^-)$	0	1	1	0	J 0 $\rightarrow$ J-1 1	$t_{0-}^J$
			2	1	1	0	J 0 $\rightarrow$ J+1 1	$t_{0+}^J$

TABLE II. Isospin factors for the  $N\bar{N} \rightarrow \pi\rho$  transition potential.

Exchange particle	Type of diagram	$I=0$	$f$	$I=1$
$N$	$s$	$-\sqrt{6}$		-2
$\Delta$	$s$	$-\sqrt{\frac{8}{3}}$		$\frac{2}{3}$
$\omega$	$t$	$-\sqrt{6}$		0

TABLE III. Coupling constants and cutoff masses for the  $N\bar{N} \rightarrow \pi\rho$  transition potential.

Vertex	$g^2/4\pi$	$\kappa$	$\Lambda$ [MeV]
$NN\pi$	14.4	-	1970
$NN\rho$	0.84	6.1	1970
$N\Delta\pi$	0.36	-	1150
$N\Delta\rho$	20.45	-	1150
$NN\omega$	19.42	-	1414

 TABLE IV. Deuteron properties predicted by the model including a soft  $\pi NN$  form factor ( $\Lambda_{\pi NN} = 1\text{GeV}$ ) and correlated  $\pi\rho$  exchange in comparison to the full Bonn potential and experiment.

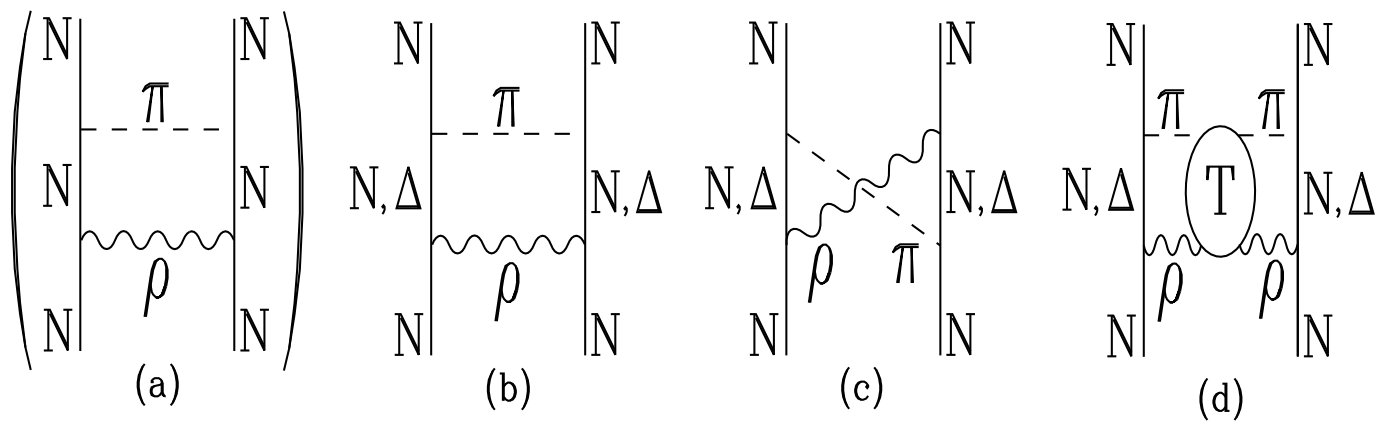
	present model	full Bonn potential	experimental data <sup>a</sup>
Binding energy $\epsilon_d$ [MeV]	2.2246	2.2247	2.2245754
D state probability $P_d$ [%]	4.37	4.25	-
Quadrupole moment $Q_d$ [ $f m^2$ ]	0.2781	0.2807	$0.2859 \pm 0.0003$
Asymptotic D/S ratio	0.0265	0.0267	$0.0271 \pm 0.0008$

<sup>a</sup>References are given in [2].

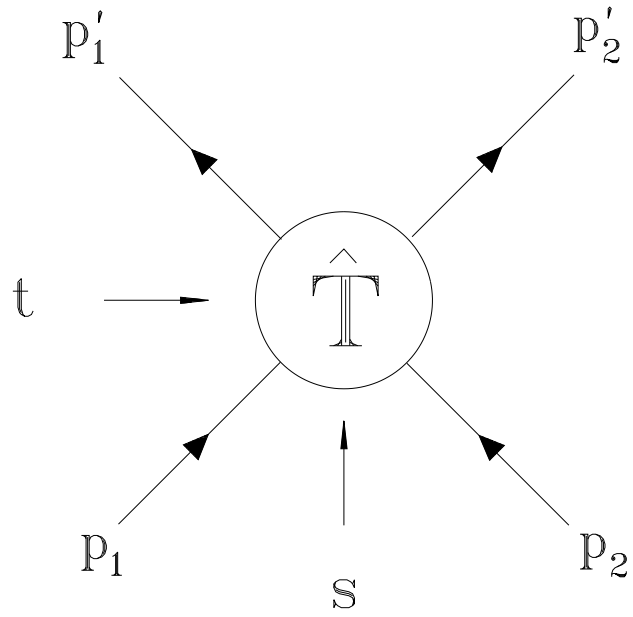
 TABLE V.  $NN$  matrix elements in helicity basis.

$\langle \lambda'_N \lambda'_{\bar{N}}   {}^J N   \lambda_N \lambda_{\bar{N}} \rangle$ ( $\lambda = \pm \frac{1}{2}$ )
${}^J N_1 \equiv \langle ++   {}^J N   ++ \rangle$
${}^J N_2 \equiv \langle ++   {}^J N   -- \rangle$
${}^J N_3 \equiv \langle +-   {}^J N   +- \rangle$
${}^J N_4 \equiv \langle +-   {}^J N   -+ \rangle$
${}^J N_5 \equiv \langle ++   {}^J N   +- \rangle$
${}^J N_6 \equiv \langle +-   {}^J N   ++ \rangle$

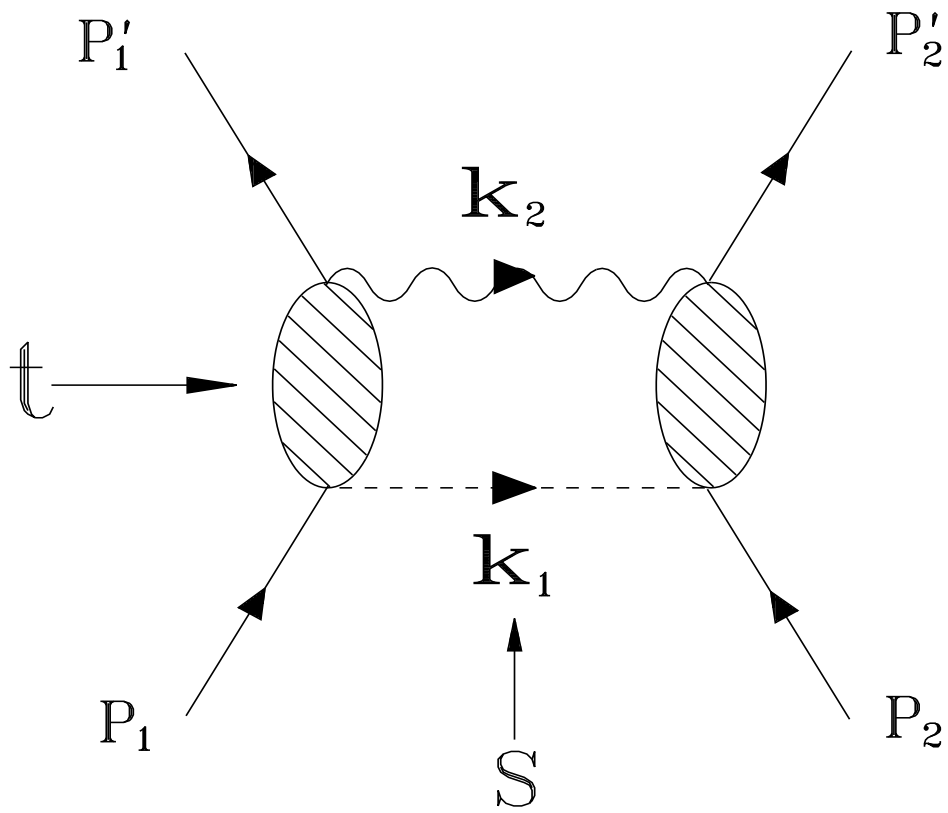




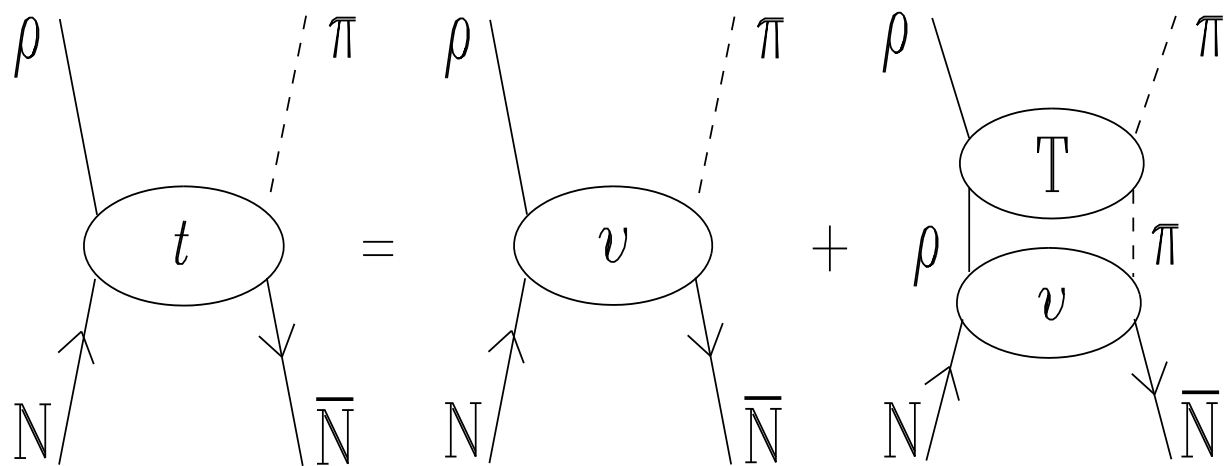
G. Janssen, K. Holinde, and J. Speth  
 Correlated ...  
 Fig. 1



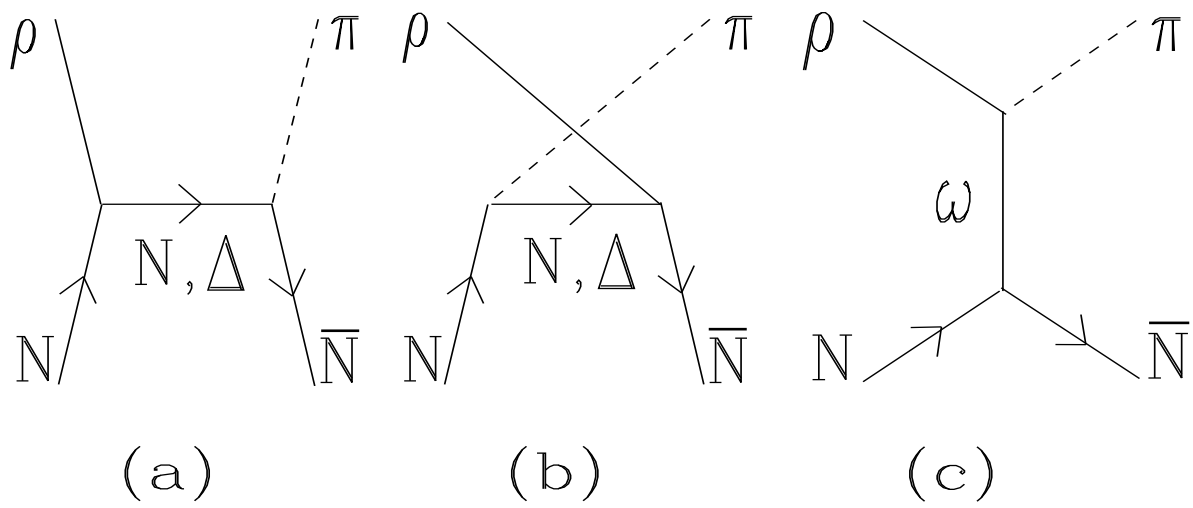
G. Janssen, K. Holinde, and J. Speth  
Correlated ...  
Fig. 2



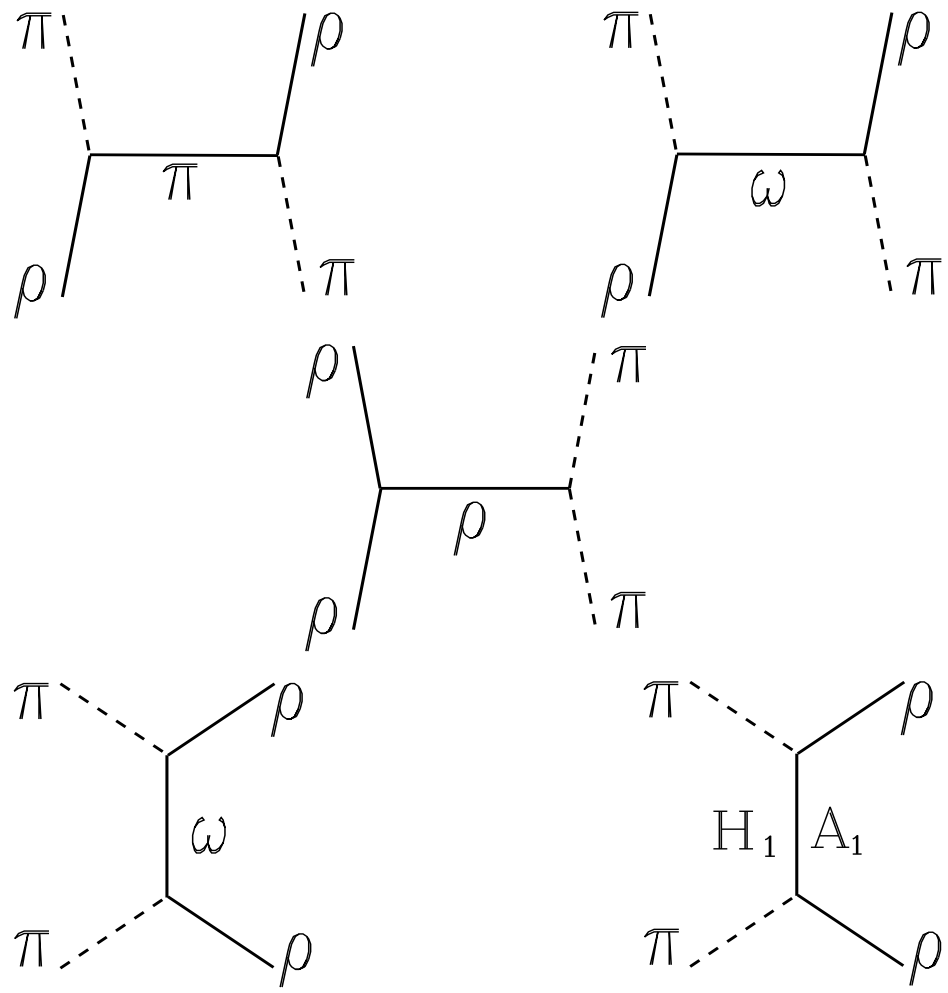
G. Janssen, K. Holinde, and J. Speth  
 Correlated ...  
 Fig. 3



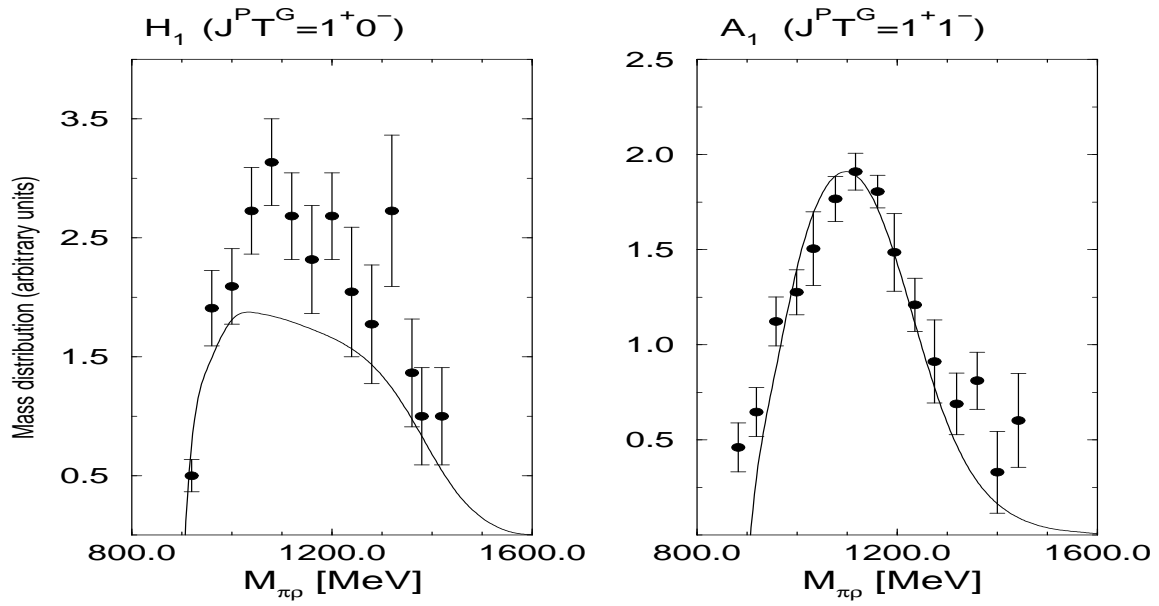
G. Janssen, K. Holinde, and J. Speth  
 Correlated ...  
 Fig. 4



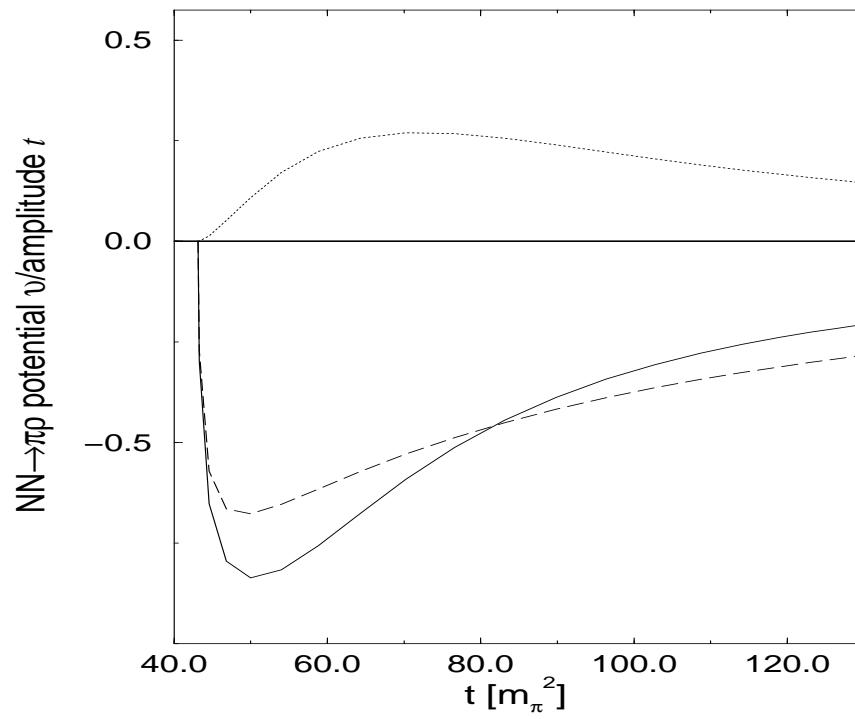
G. Janssen, K. Holinde, and J. Speth  
 Correlated ...  
 Fig. 5



G. Janssen, K. Holinde, and J. Speth  
 Correlated ...  
 Fig. 6

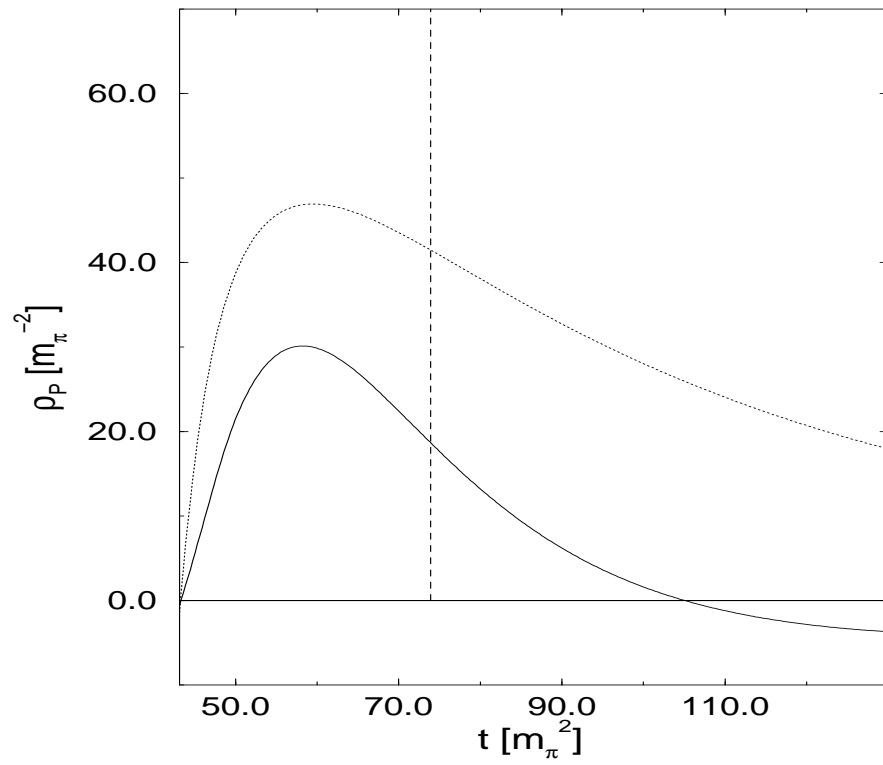


G. Janssen, K. Holinde, and J. Speth  
Correlated ...  
Fig. 7

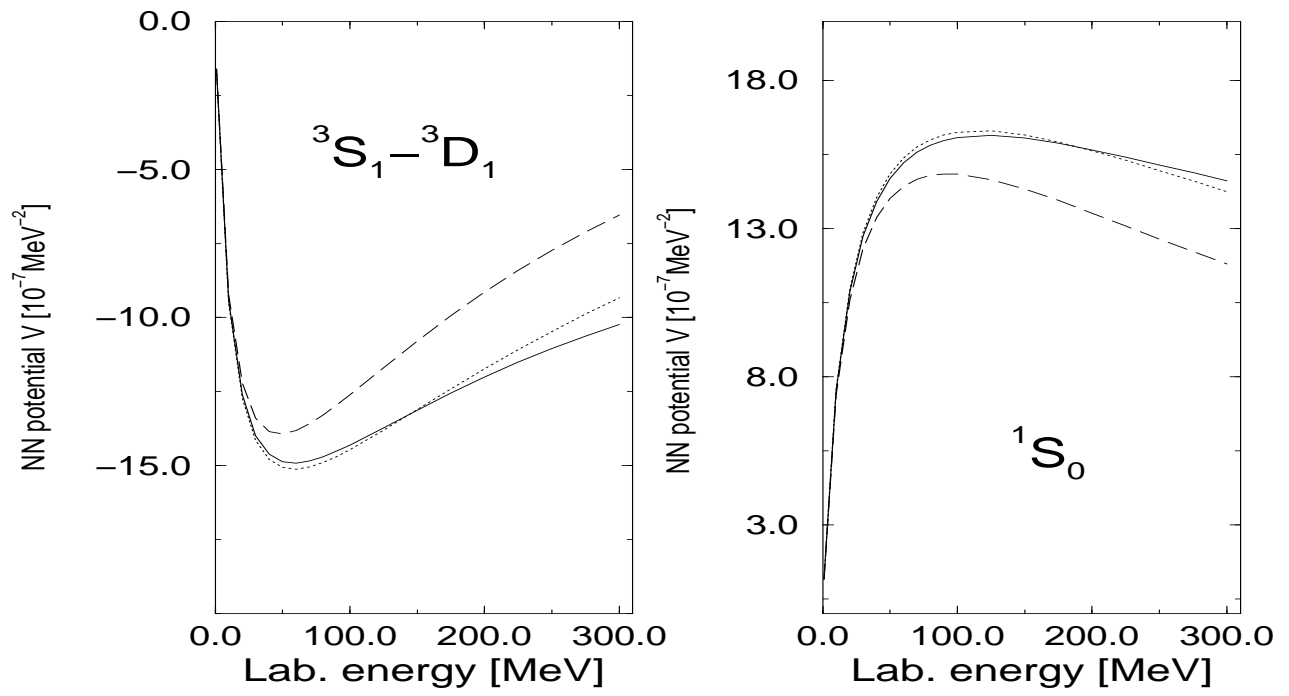


G. Janssen, K. Holinde, and J. Speth  
Correlated ...  
Fig. 8

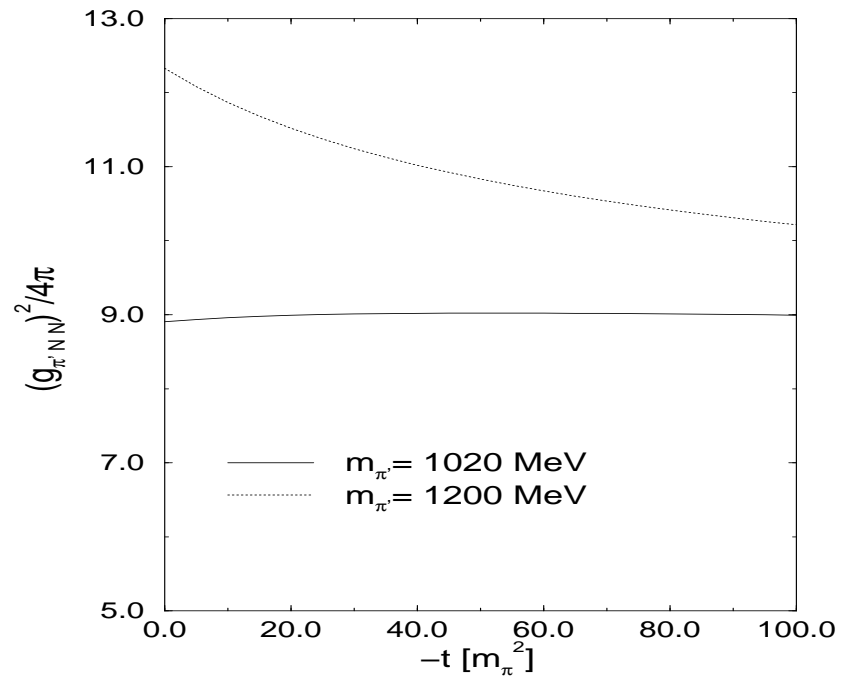




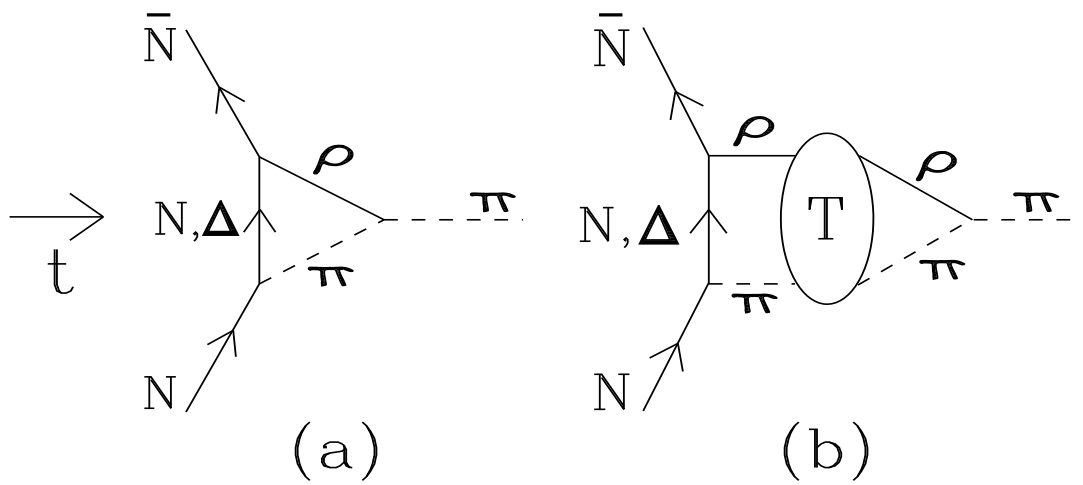
G. Janssen, K. Holinde, and J. Speth  
Correlated ...  
Fig. 9



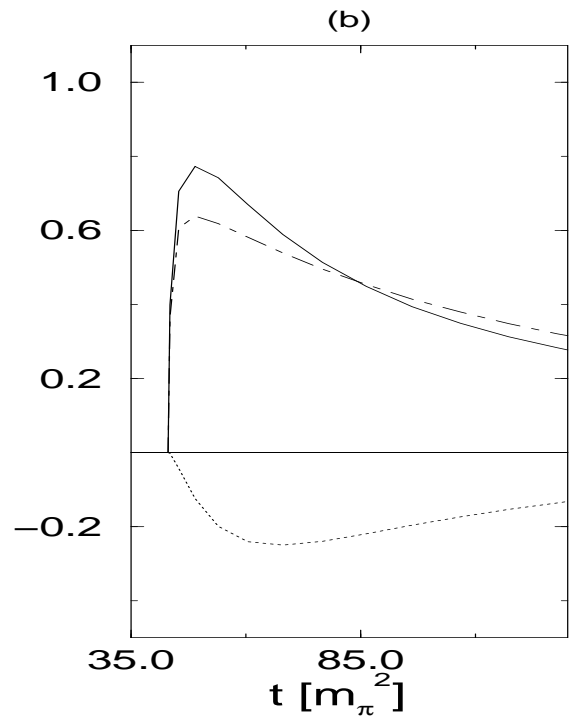
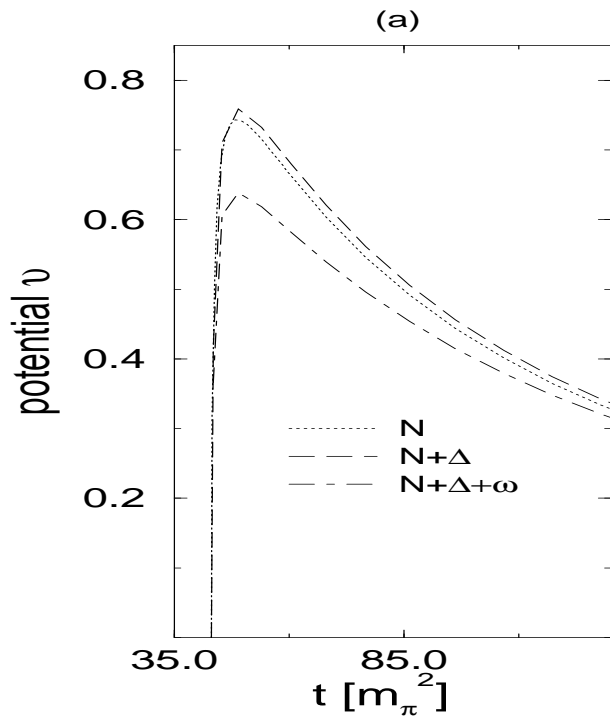
G. Janssen, K. Holinde, and J. Speth  
 Correlated ...  
 Fig. 10



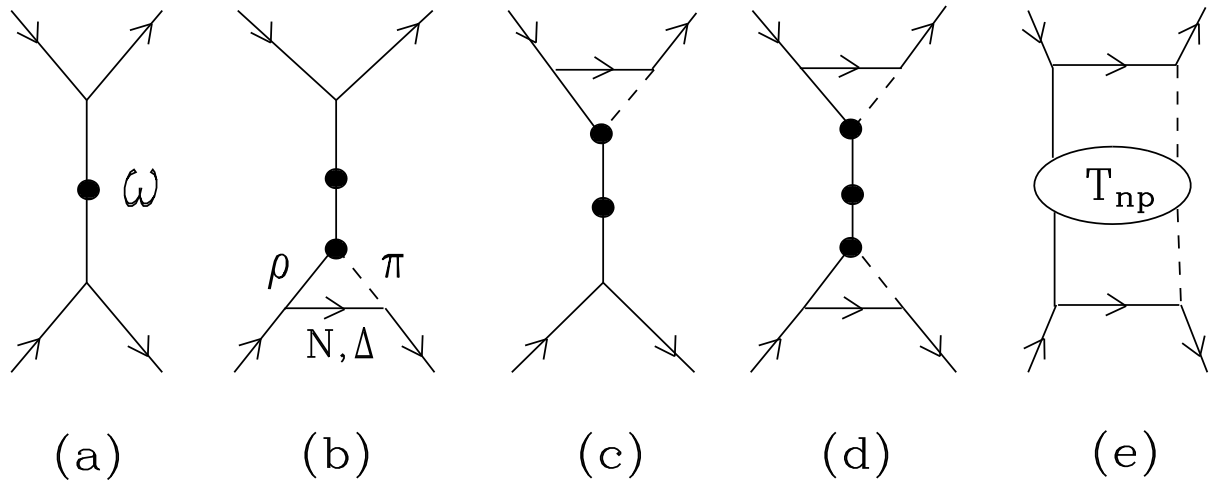
G. Janssen, K. Holinde, and J. Speth  
Correlated ...  
Fig. 11



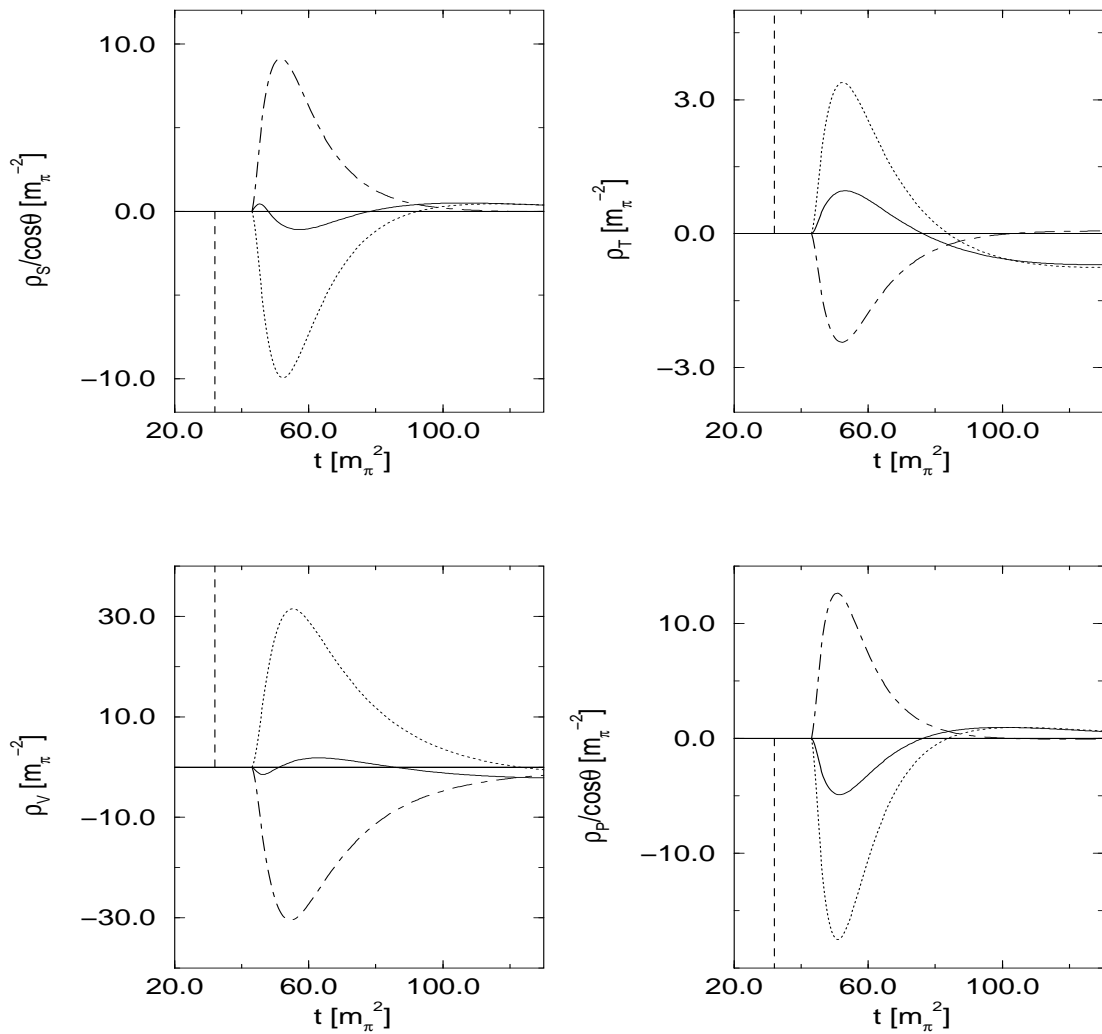
G. Janssen, K. Holinde, and J. Speth  
 Correlated ...  
 Fig. 12



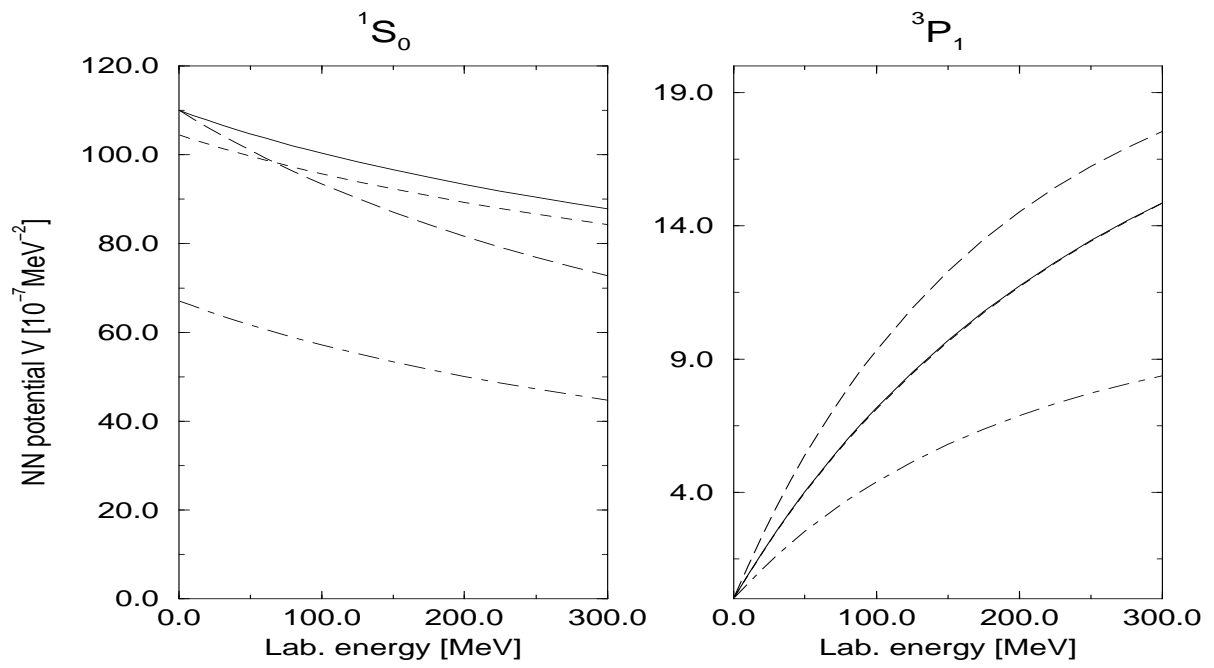
G. Janssen, K. Holinde, and J. Speth  
Correlated ...  
Fig. 13



G. Janssen, K. Holinde, and J. Speth  
 Correlated ...  
 Fig. 14

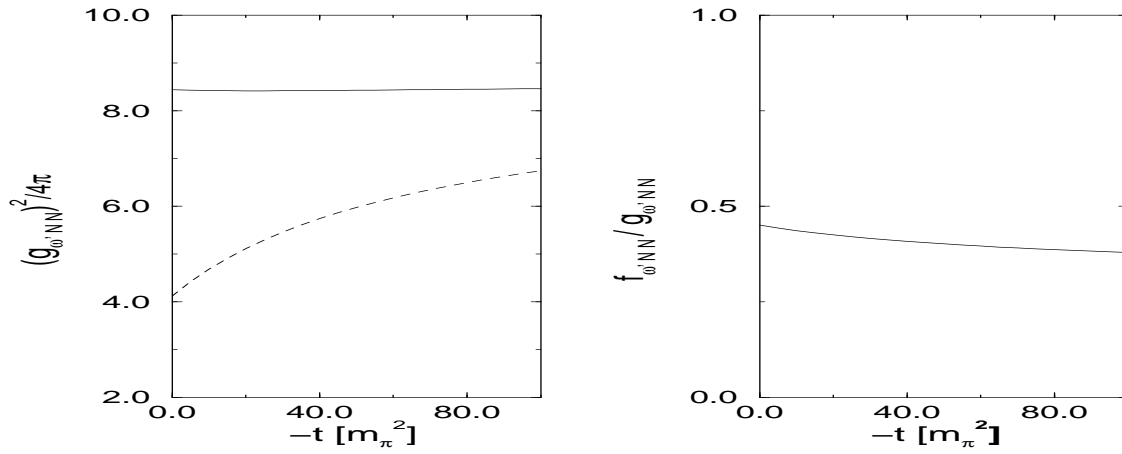


G. Janssen, K. Holinde, and J. Speth  
 Correlated ...  
 Fig. 15

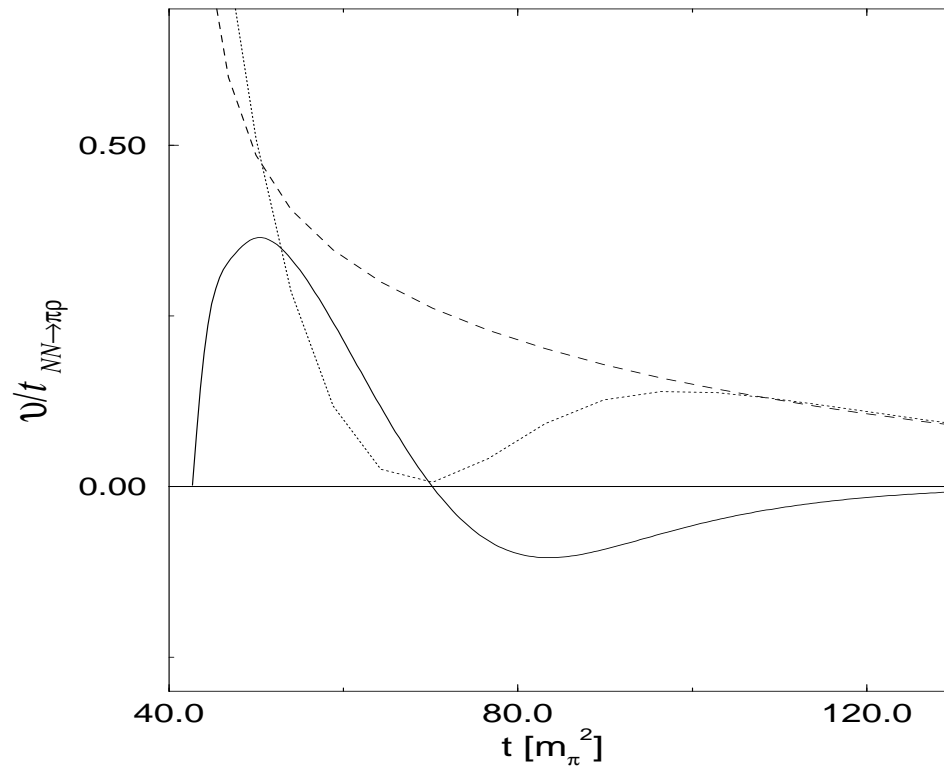


G. Janssen, K. Holinde, and J. Speth  
Correlated ...  
Fig. 16

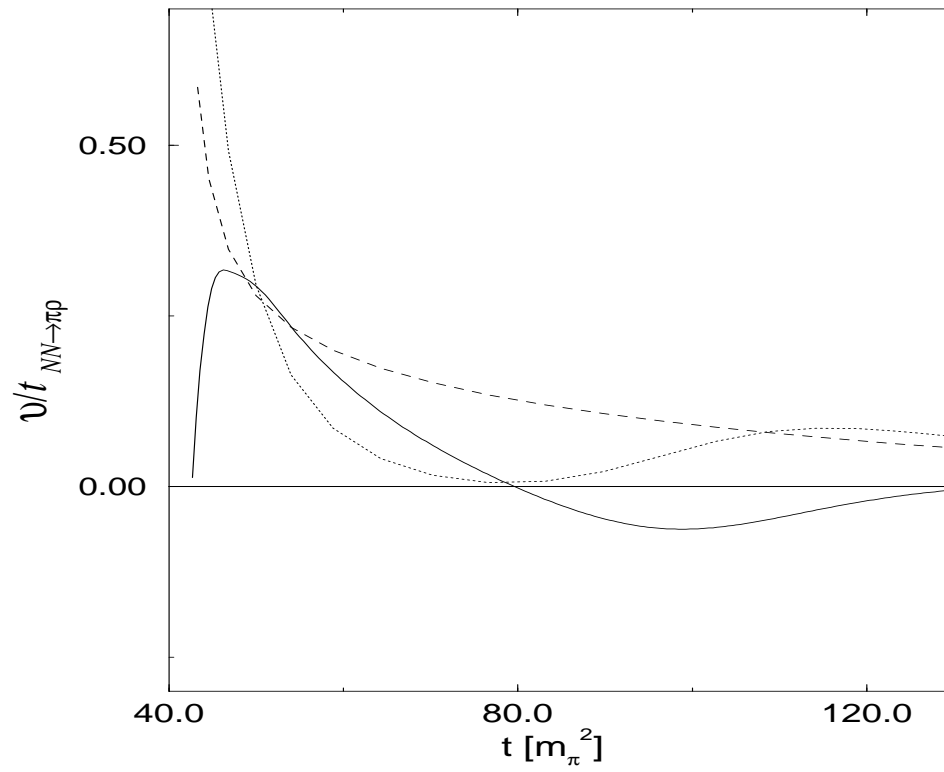




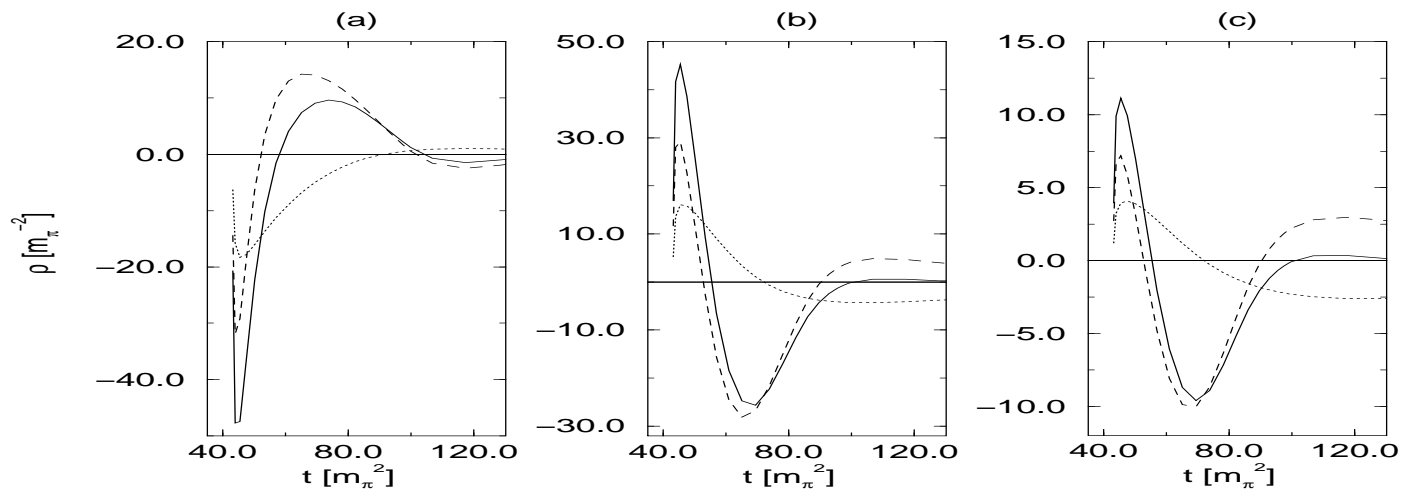
G. Janssen, K. Holinde, and J. Speth  
Correlated ...  
Fig. 17



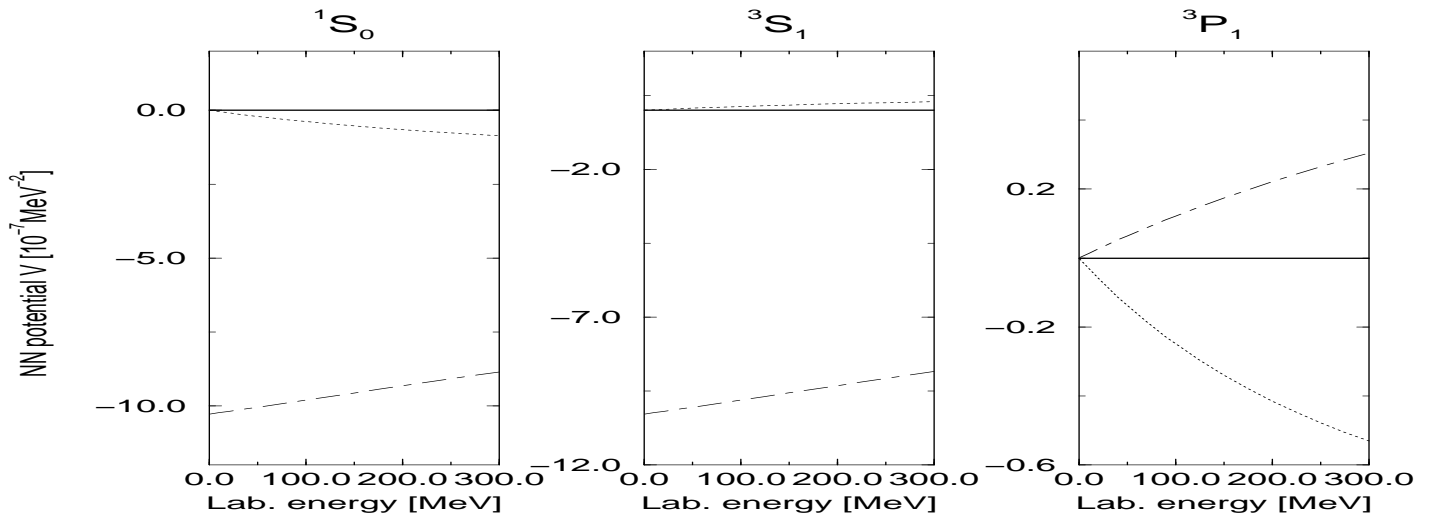
G. Janssen, K. Holinde, and J. Speth  
Correlated ...  
Fig. 18



G. Janssen, K. Holinde, and J. Speth  
Correlated ...  
Fig. 19



G. Janssen, K. Holinde, and J. Speth  
Correlated ...  
Fig. 20



G. Janssen, K. Holinde, and J. Speth  
 Correlated ...  
 Fig. 21